UNIVERSITÀ DEGLI STUDI DI PADOVA

DIPARTIMENTO D' INGEGNERIA INDUSTRIALE

e

DIPARTIMENTO DI TECNICA E GESTIONE DEI SISTEMI INDUSTRIALI

Corso di Laurea Magistrale in INGEGNERIA MECCANICA

TESI DI LAUREA

EFFETTO DEL FOSFORO SUL SILICIO PRIMARIO NELLE LEGHE AL-SI IPEREUTETTICHE

Relatore: Chiar.mo PROF. FRANCO BONOLLO

Correlatori: Chiar.mo PROF. SSA MARISA DI SABATINO

Laureando: ZAMBON ALESSIO

ANNO ACCADEMICO 2015-2016

Table of contents

1 Introduction 6
1.1 Purpose of the thesis 6
1.2 Sites and people involved 6
2 Alloys examined 6
2.1 Al – Si System 6
2.1.1 Al – Si hypereutectic alloys [5] 9
2.1.2 Primary silicon 12
2.1.3 Mechanical properties Applications of hypereutectic Al-Si alloys 14
2.2 Al – Si – Cu alloys 17
2.2.1 Al – Si – Cu System 17
2.3 Refinement of primary Si 18
2.3.1 Generality 18
2.3.2 Al-3P master alloy 20
2.3 X-ray technique (Micro focus X-ray radiography) 22
4 Experimental 24
4.1 Casting 24
4.2 Preparation of the samples 29
4.3 Chemical analysis 30
4.4 Light microscope 31
4.5 In-situ X-ray radiographic study 32
5 Results and discussion 35
5.1 Cooling curves and liquidus temperatures 35
5.1.1 Alloy prepared by commercial pure Al alloys 35
5.1.2 High pure raw material 38
5.2 Chemical analysis 39
5.3 Light microscope pictures 40
5.3.1 Size and shape of the primary silicon particles 40
5.3.2 Floating effect 48
5.4 Image sequences of in-situ X-ray radiographic study 49
6 Conclusion 54

Bibliography 55

1 Introduction

1.1 Purpose of the thesis

The following thesis has the main purpose of studying the effect of phosphorus on the modification of primary silicon phase in hypereutectic Al-Si alloys. In particular we studied how the nucleation and growth of primary silicon is influenced by the modification with addition of different amounts of phosphorus under different cooling conditions, in terms of cooling rates. This is important because a fine primary silicon structure is favorable for the casting properties and mechanical properties of hypereutectic Al-Si alloys.

1.2 Sites and people involved

Research work and experiments were conducted at NTNU Gløshaugen buildings in Trondheim under the supervision of professor Yanjun Li and professor Marisa Di Sabatino, and in collaboration with PhD candidate, Yijiang Xu. The Italian relator was professor Franco Bonollo.

2 Alloys examined

2.1 Al – Si System

Among aluminum casting alloys, aluminum–silicon (Al–Si) alloys containing silicon as the major alloying element comprise more than 90 % of the total aluminum castings produced wordwide and have wide applications, especially in the transportation industry. This dominance of Al–Si alloys among aluminum foundry products can be attributed to their excellent castability, crack resistance and good mechanical properties achieved. In general the content of silicon in the Al–Si alloys varies from 4 to 25 wt. % Si. The phase diagram (at 1 atm of pressure, fig.1): the eutectic point at 12.6 wt.% of Si at 577 °C. Once the Si content is higher than 12.6 wt.%, Si crystal will form as the primary phase during the solidification of binary Al-Si alloy. Hyper eutectic Al-Si alloys are widely used in wear-resistance applications, for example pistons in engines. Moreover the figure shows that at room temperature Si has extremely low solubility in Aluminum, but it increases with increasing temperature and reaches the maximum value of l 1.65 wt. % at 577 °C.

This project is focusing on the solidification of hyper eutectic Al-Si alloys. The Si content is selected as 18 wt. % in the experimental alloys, which is a typical content in many commercial hyper eutectic alloys. Such a Si content is also favorable to control the liquidus temperature of the alloys to relatively low temperatures for the ease of in-situ X-ray radiographic study.

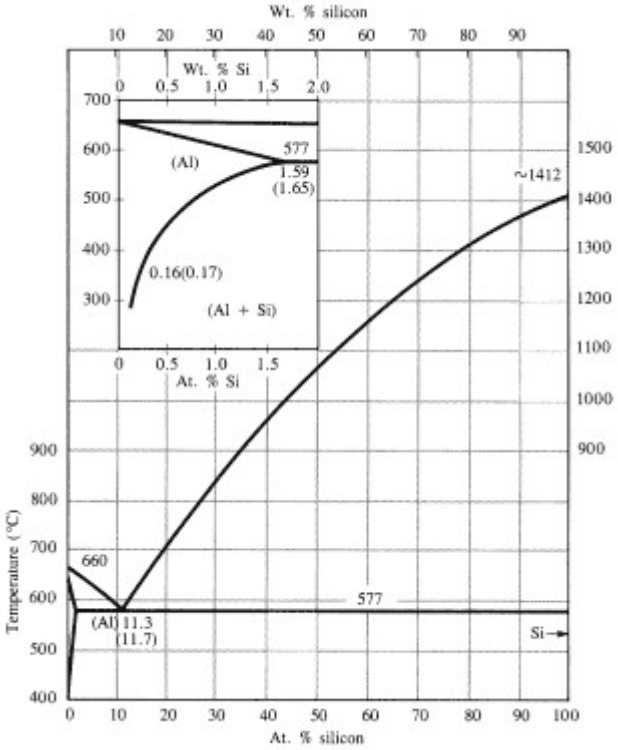

Figure 1 Phase diagram of Al – Si

As shown below (fig.2) , here are the different microstructures that we may obtain, as a function of % Si: on the left the hypoeutectic one, in the middle eutectic one and on the right hypereutectic one.

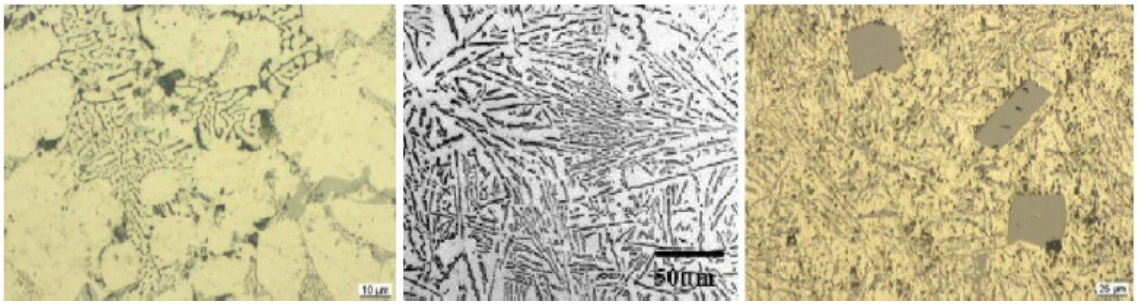

Figure 2 Different microstructures of Al-Si alloys [2]

In order to understand the role of Phosphorus modification, it is also important to study the primary Silicon in alloys without modification. The primary silicon crystals in untreated alloys have coarse hexagonal and long plate-like shape as better shown in fig.3. [2,3]

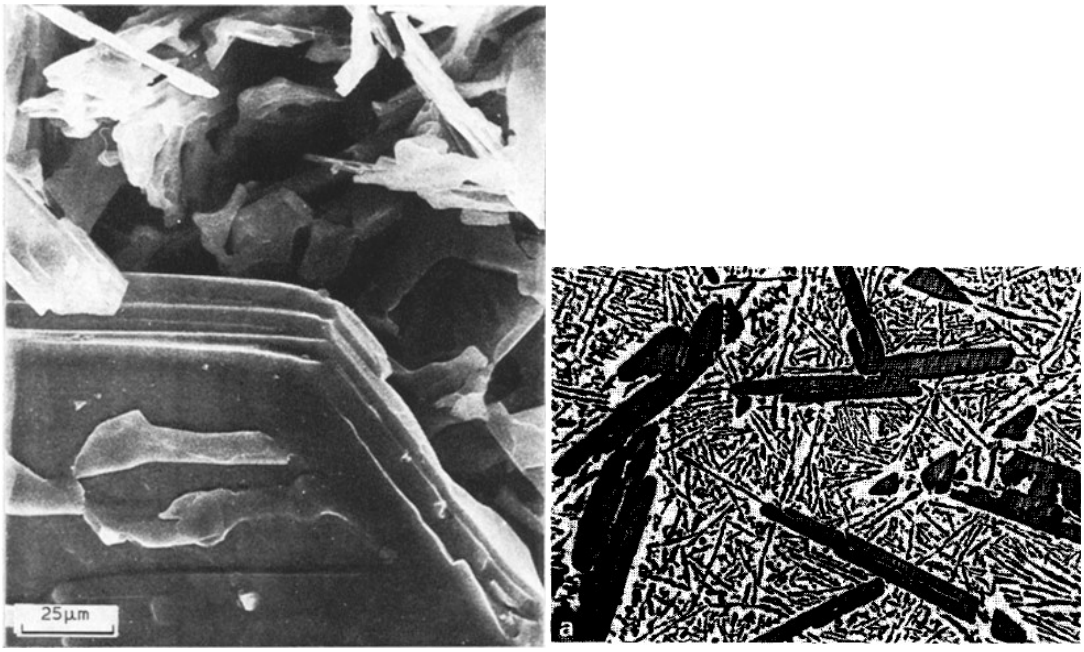

Figure 3 Plate of primary Silicon: on the left a tridimensional imagine of primary silicon particles into the aluminum matrix, and on the right a two-dimensional imagines with primary and eutectic silicon into aluminum matrix. [3]

This morphology of primary Si is detrimental to mechanic properties because they are faced with inhomogeneous structure with a large amount of point trigger crack.

For hypoeutectic Al-Si alloys, Silicon gives good proprieties for casting processes because with a higher content of Si the fluidity of the alloy increases. This is the main reason why the Silicon is used as a main alloying element for casting alloys because thanks to this the liquid alloys fill more easily the molds and it decreases the problems caused by solidification shrinkage (fig.5), that could be halved by the silicon, because the fluid is more free and it can pass better through the material already solidified. The increase of the fluidity depends on the rate of Silicon as shown in fig. 4 [4]. This figure shows the results of an experiment in which a special spiral mold was filled with different Al – Si alloys; the Y axis reports how many millimeters of the mold the liquid is able to fill.

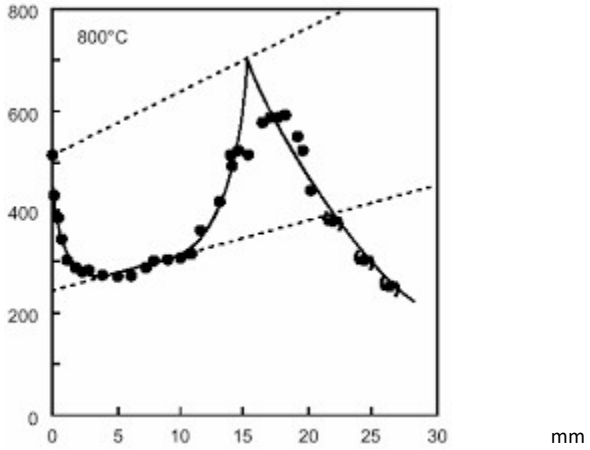

Figure 4 Fluidity of alloys understood as millimeter of penetration in a particular spiral mold against %Si [4].

As it can be seen the best fluidity and consequently the best castability occurs around 16% of silicon or at very pure aluminum, but it is not relevant for this study.

Al puro	8.0 %
Al-4%Cu	8.8 %
Al-4%Cu-2%Ni-Mg	5.3 %
Al-5%Cu	6.0 %
Al-5%Zn-Mg	4.7 %
Al-1%Mg-Si	4.7 %
Al-5%Mg-Si	6.7 %
Al-5%Si-1%Cu	4.9 %
Al-5%Si-2%Cu	5.2 %
Al-5%Si-2%Cu-Mg	4.2 %
Al-7%Si-Ni-Mg	4.5 %
Al-7%Si-2%Cu-Mg	6.5 %
Al-12%Si	3.5 %

Figure 5 Table with % for various alloys with different % of Silicon [4].

2.1.1 Al – Si hypereutectic alloys [5]

Al–Si alloys with silicon content more than 13 % are termed as hypereutectic alloys fig.6

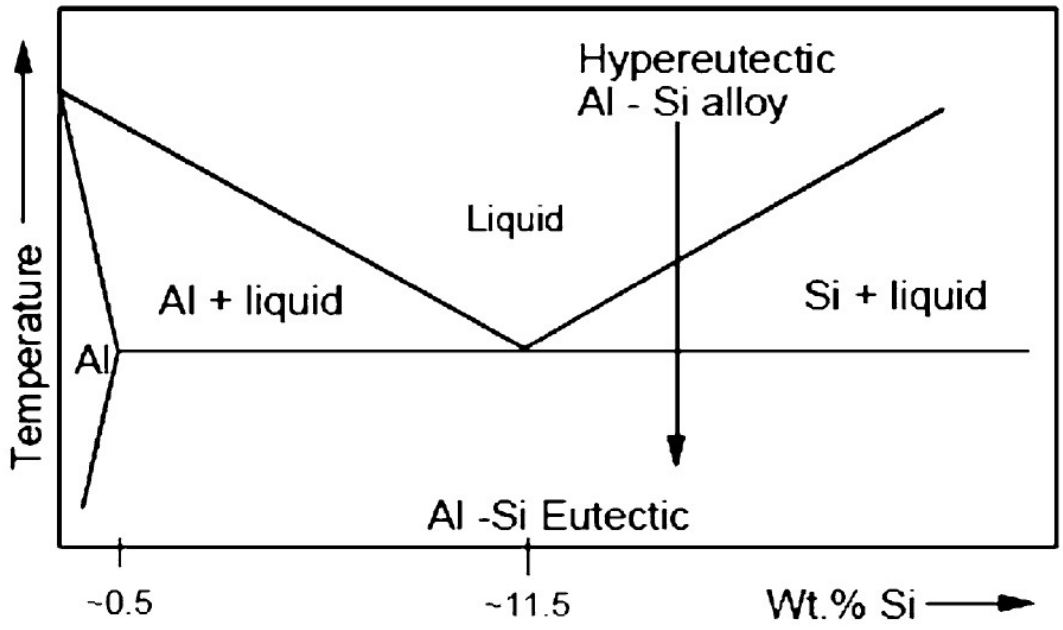

Figure 6 Phase diagram of Al-Si System with the hypereutectic region [5].

In this region, when cooling from the liquid phase the alloys have different transformations during solidification:

- According to phase diagram the first solid phase that appears is primary silicon as primary particles, floating in liquid of silicon and aluminum;
- During further cooling, the primary Si particles will grow by consuming the silicon from the liquid, moving the composition of the liquid towards the eutectic point;
- When it reaches the eutectic temperature, that is 660,32 °C for Al-Si systems, the remaining liquid composed of 12.6 % of silicon transforms in eutectic solid phase
- The final result is: some primary silicon particles inside a eutectic matrix, fig.7

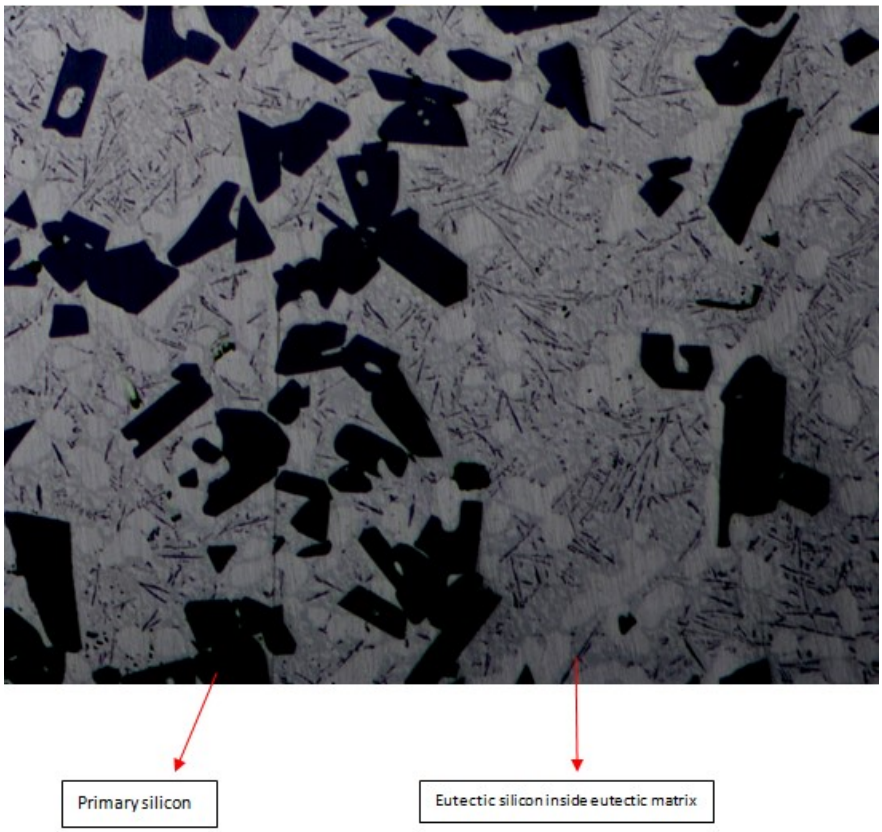

Figure 7 Final structure in an hypereutectic alloy.

Hypereutectic Al–Si alloys have low density, high specific stiffness, high-temperature resistance, wear resistance, and low coefficient of thermal expansion and therefore are interesting for several applications and this proprieties are mostly due to primary silicon. The properties of the hypereutectic alloy are greatly dependent on the morphology, size and distribution of primary silicon crystals in the alloy, and these aspects will be investigated later.

The main commercial alloys are shown in Tab. 1, with their compositions and with their principal applications [11].

Table 1 Hypereutectic Al-Si Alloy Designations and Nominal Compositions [11].

Designation	Owner	Si	Cu	Mg	Fe	Ni	Others		Applications	Notes
LM28	BS1490:1988	18	1.5	1		1		Nom.	Pistons	
LM28	BS1490:1988	17 - 20	1.3-1.8	0.8-1.5	≤0.7	0.8-1.5	≤0.6Mn, ≤0.2Zn, ≤0.1Pb, ≤0.1Sn, ≤0.2Ti, ≤0.6Cr, ≤0.5Co, ≤0.1Others (each), ≤0.3 Others (total)	Spec.		
LM29	BS1490:1988	23	1	1		1		Nom.	Pistons	
LM29	BS1490:1988	22 - 25	0.8-1.3	0.8-1.3	≤0.7	0.8-1.5	≤0.6Mn, ≤0.2Zn, ≤0.1Pb, ≤0.1Sn, ≤0.2Ti, ≤0.6Cr, ≤0.5Co, ≤0.1Others (each), ≤0.3 Others (total)	Spec.		
LM30	BS1490:1988	17	4.5	0.5				Nom.	Linerless engine blocks	
LM30	BS1490:1988	16 - 18	4-5	0.4-0.7	≤1.1	≤0.1	≤0.3Mn, ≤0.2Zn, ≤0.1Pb, ≤0.1Sn, ≤0.2Ti, ≤0.1Others (each), ≤0.3 Others (total)	Spec.		
Alusil	KS Aluminium Technologie AG	17	4	1				Nom.	Linerless engine blocks (Porsche Cayenne, Audi V6 and V8, BMW)	
A390	Al Assoc.	17	4.5	0.6	<0.4		0.5Zn	Nom.	Primary sand and permanent mould alloy. For die castings 390 is used (higher Fe content to prevent die-soldering).	
B390	Al Assoc.	16 - 18	4-5	0.45-0.65	<1.3	<0.1	<0.5Mn, <1.5Zn, <0.2Ti, ≤0.1Others (each), ≤0.2 Others (total)		Engine blocks, pistons, pumps, compressors. Secondary (scrap-based) alloy. Workhorse alloy 99.5% of all 390 series applications)	
391 (Mercasil)	Mercury Marine	18 - 20	<0.2	0.4-0.7	<1.2		<0.3Mn		Die-casting. Marine Engine Blocks (low Cu to improve corrosion resistance). A391 for permanent mould (<0.4Fe). B391 for sand casting (<0.2Fe)	
393 (Vanasil)		21 - 23	0.7-1.1	0.7-1.3	<1.3	2.0-2.5	<0.1Mn, <0.1Zn, 0.1-0.2Ti, 0.08-0.15V, ≤0.15 Others (total)		Diesel pistons. Very early hypereutectic alloy (introduced more than 50 years ago), and continues to be used.	
DISPAL S250	Peak	20			5	2		Nom.	Cylinder liners	Spray formed
DSIPAL S260	Peak	25	4	1				Nom.	Cylinder liners	Spray formed
MSFC-398	NASA								Pistons	
M174+	MAHLE								Pistons	

2.1.2 Primary silicon

Primary Si in hypereutectic Al-Si alloys exhibits a variety of morphologies such as star-like, polygonal, coarser platelet, etc. Generally, the machinability of hypereutectic Al-Si alloys is worse due to the presence of coarser primary Si. Ullah et al. [12] studied the silicon crystal morphologies formed during solidification of Al-Si alloys containing 17-38 wt% Si; they found that at lower silicon contents the silicon morphologies have a fish-bone or star-like shape but at higher Si contents the morphology changed to large plates that have a tendency to grow in layers and thus have Al as inclusions in the Si crystals. Examples of these primary Si morphologies are shown in fig 8.

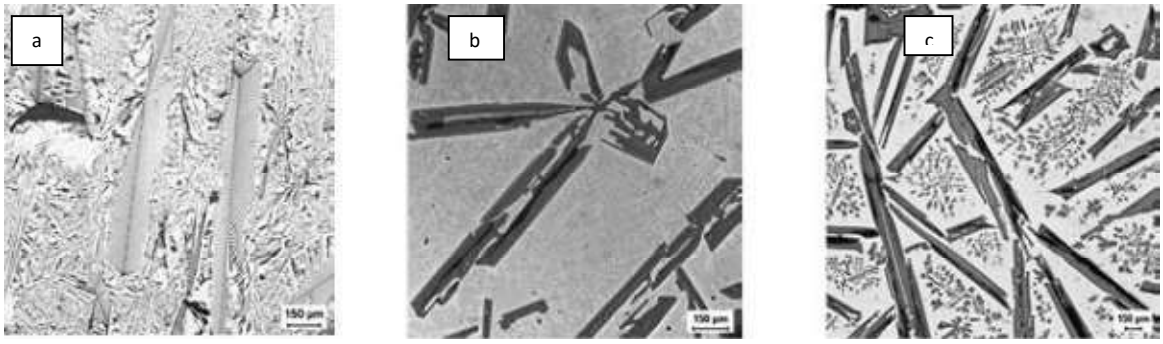

Figure 8 Primary silicon crystal morphologies: (a) Fish-bone-like structure, (b) Large star shaped crystal and (c) Large plate structure [12].

The strong tendency of Si to grow in the (111) plane through the twin plane re-entrant angle edge mechanism (TPRE) combined with different nucleation conditions is the reason for the formation of the different morphologies. However, at increasing super saturation a specific type of hopper crystal grows, where the edges and corners grow fast, which, together with the preferred growth in the (111) plane, results in the five-fold star. Figure 9 shows SEM micrographs of five-fold primary Si crystals.

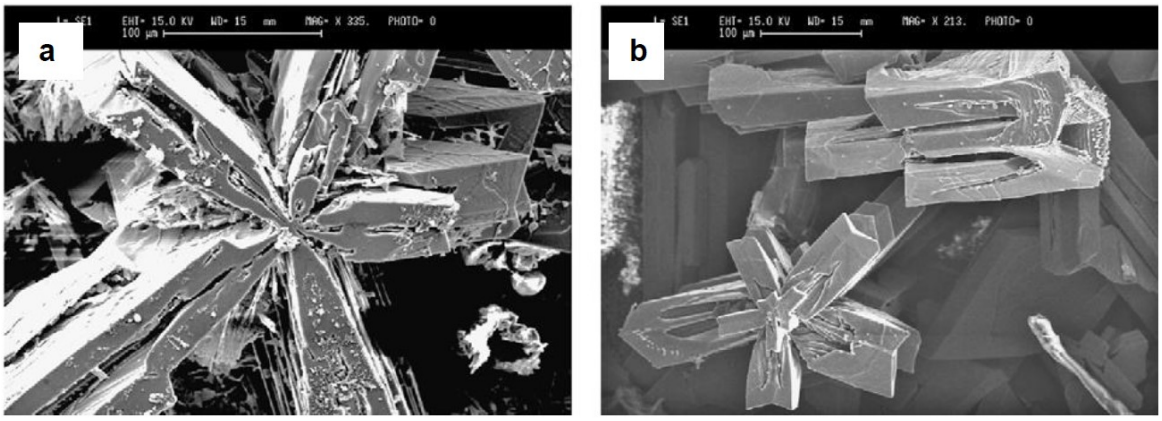

Figure 9 SEM micrographs of star shaped crystals in Al-25wt%Si alloy: (a) fully developed star with five arms growing in length and thickness from a common nucleus; (b) a star crystal at an early stage of development [12].

Xu and Jiang [13] concluded that the morphologies of primary Si are a strong function of the solidification conditions such as melt superheat and cooling rate. As the melt temperature increases, the morphologies of primary Si change from star-like and other irregular primary Si to octahedral primary Si and the size of primary Si will gradually decrease. Also they found that the cooling rate plays an important role in determining the morphologies of primary Si in the solid state. The size of primary Si will gradually decrease with increasing cooling rate. In general, the size of the primary Si increases with increasing Si content and with decreasing cooling rate. Larger superheating seems to promote the formation of the fish bone structure.

It has been reported that high melt superheating and quick cooling to a pouring temperature could significantly refine the primary Si of Al-Si alloys without addition of refinement elements and the microstructure in the solid state is influenced by the liquid structure before solidification.

Li et al. investigated the effect of cooling rate and superheat on Si morphology. Al-16wt%Si alloy was heated to 720, 880, 960 and 1050 °C and then cooled to 720°C in air (at 60-70 K/s) and cast into sand and metal molds. Also, the alloy was cooled back to 720 °C at 150-200 K/s (by adding solid samples to the melt) and cast into metal moulds. In each case the primary Si show greater refinement (and a more compact morphology) with increasing melt superheat. The effect was more dramatic in the sand castings than in the metal mold castings, the latter being more refined as a result of the higher solidification rate in the metal molds, although the primary Si was always more refined in the metal mold castings than in the sand castings. Greater refinement was also achieved by cooling from the superheated temperature to the pouring temperature at a higher rate. Their explanation for the refinement process was not enough.

2.1.3 Mechanical properties Applications of hypereutectic Al-Si alloys

The hypoeutectic and hypereutectic Al-Si alloys have both been used as tribological material in engine applications. However, hypereutectic Al-Si alloy can be used to produce engine block without cylinder liner as it has a higher wear resistance resulting from a larger fraction of silicon phase. Usually, the hypereutectic Al-Si alloy engine block surface is electrochemically treated to etch away some of the matrix aluminum so that the eutectic and primary silicon particle can protrude to sustain wear. The general mechanism responsible for such an increase in the wear resistance of Al-Si alloy is that silicon increases the overall hardness of the alloy and thus makes it more resistant to wear. However, this does not always mean that the higher the fraction of silicon in the alloy, the greater the wear resistance is. Due to its high brittleness, impact load can break silicon and thus may increase the overall wear of the alloy. This is especially true when the silicon phase has a coarse morphology. So the optimal fraction of silicon in Al-Si alloy relies on the service condition and silicon morphology of the material.

Al–Si hypereutectic alloys possess low thermal expansion, excellent castability and low density which make them attractive for automotive and aerospace applications. Al–Si hypereutectic alloys are widely used to produce engine blocks and cylinder liners, which is a good replacement of cast iron, by which the weight of automotive can be greatly reduced.

Figure 10 Engine block and aluminum piston

The major applications of hypereutectic Al–Si alloy also include high-performance automobile engine parts such as connecting rods, rocker arms, cylinder (fig.10), pistons, valve retainers. Some of these alloys used in this field are called with different name like Alusil, Lokasil, Silitec, DiASil, Mercosil.

The good wear-resistance and low thermal expansion of hypereutectic Al-Si alloys are due to the primary silicon precipitated during solidification, which are dependent on the morphology and distribution of primary Si in the matrix. The best results are achieved with a fine and well dispersed particles of primary silicon. Thus we have to control the size of these particles of silicon which are directly influenced by cooling rate and melt temperature; particularly higher melt temperatures and increase in cooling rates resulted in positive effect on the size and the distribution of primary silicon. In addition, this refinement of primary silicon can be achieved with modification of phosphorus, and this will be the aim of our studies that will be shown in the next chapters. Moreover increasing the percentage of silicon we will obtain a more light cast thanks to less specify weight of silicon. With this large amount of silicon we can also reduce even more the volume decreasing on solidification due to shrinkage of Al crystals.

But primary silicon is also the problem of this type of alloys because it is the first solid part that appears and having less density than the liquid (this is even more serious for Al-Si-Cu alloys because Cu will increase the density of liquid). The primary Silicon crystals will float in the liquid, provoking macro segregations in the casting. Thus we have to find a way to homogenize the liquid during the solidification and reduce the dimensions of this primary silicon. The last problem that occurs only with an

appreciable amount of Cu, is the low corrosion resistance especially in a salt water environment and this will be a problem for the big naval engine.

Therefore the hypereutectic alloys can reach very good mechanical properties with a good wear resistance if we can manage the shape and size of primary Silicon.

The primary silicon particles increase a lot the wear resistance of Al-Si alloys thanks to their high hardness. The major mechanism responsible for the wear of Al-Si alloys is the delamination of surface material. The breaking of silicon particles or the interfaces between silicon and matrix can initiate microcracks [14]. These microcracks propagate along the subsurface until they reach the surface, where the whole piece of material is removed. Simultaneously, external abrasives can cut off the soft aluminum matrix by local plastic deformations, if there is no protection from the secondary hard phase. Silicon particles have been found to be important to the wear resistance of Al-Si alloy. At a relatively low load, wear resistance is not strongly affected by the silicon content. However, as the load increases, addition of silicon into Al-Si alloy increases the wear resistance fig.11. Both the transition loads from mild wear to intermediate wear and from intermediate wear to severe wear of the Al-Si alloy increase with the increase in silicon content.

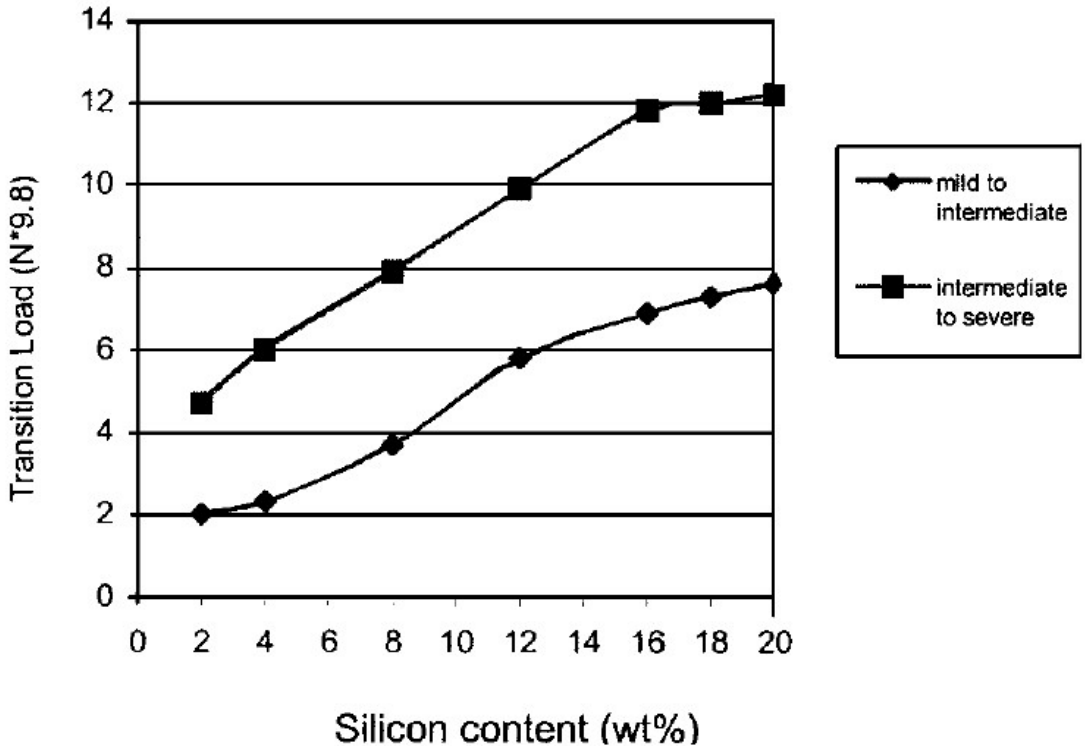

Figure 11 Influence of silicon content on wear resistance of Al-Si alloy[14].

2.2 Al – Si – Cu alloys

2.2.1 Al – Si – Cu System

Due to its importance in industry, ternary Al–Cu–Si alloys have been heavily investigated over the last decades. Al–Cu–Si alloys are, for example, of growing importance for automotive industry due to its lightweight. The ternary alloys show higher strength than Al–Si alloys and their corrosion resistance is better than in Al–Cu alloys [1]. For designing ternary alloys matching specific requirements, fundamental understanding of the phase relationships and solidification behavior is essential. The Cu-rich corner of Al–Cu–Si and even of the binary subsystems Al–Cu and Cu–Si, are highly complex. Despite various studies of phase equilibria the ternary system is still not fully understood. [16].

The Al-Cu-Si phase diagram can be used to correctly analyze the phase composition of casting alloys of 3XX.0 and 2XX.0 series with low concentrations of iron and magnesium impurities. It is also required for the analysis of more complex phase diagrams involving Cu and Si. No ternary compounds are formed in the aluminum corner of the Al-Cu-Si system. The phases Al_2Cu and (Si) are in equilibrium with the aluminum solid solution. The Al_2Cu phase has a tetragonal structure with lattice parameters a = 0.6063 nm, c = 0.4872 nm. This phase exists in a homogeneity range of 52.5-53.9% Cu which does not reach the stochiometric concentration of copper (54.2%). The density of this phase in binary alloys is 4.34 g/cm^3.

The solubility of copper in silicon and silicon in Al_2Cu are negligibly small. The maximal solubility of copper and silicon in Al crystal at the eutectic temperature (525°C) is 4.5% Cu and 1.1% Si. As the temperature lowers, the solubility of these elements in Al decreases. Under real solidification conditions, eutectic particles of the Al_2Cu and Si phases are formed at smaller concentrations of copper and silicon. The distribution of phase regions in the as-cast state depends on the cooling rate. The phase diagram is shown in Fig. 12:

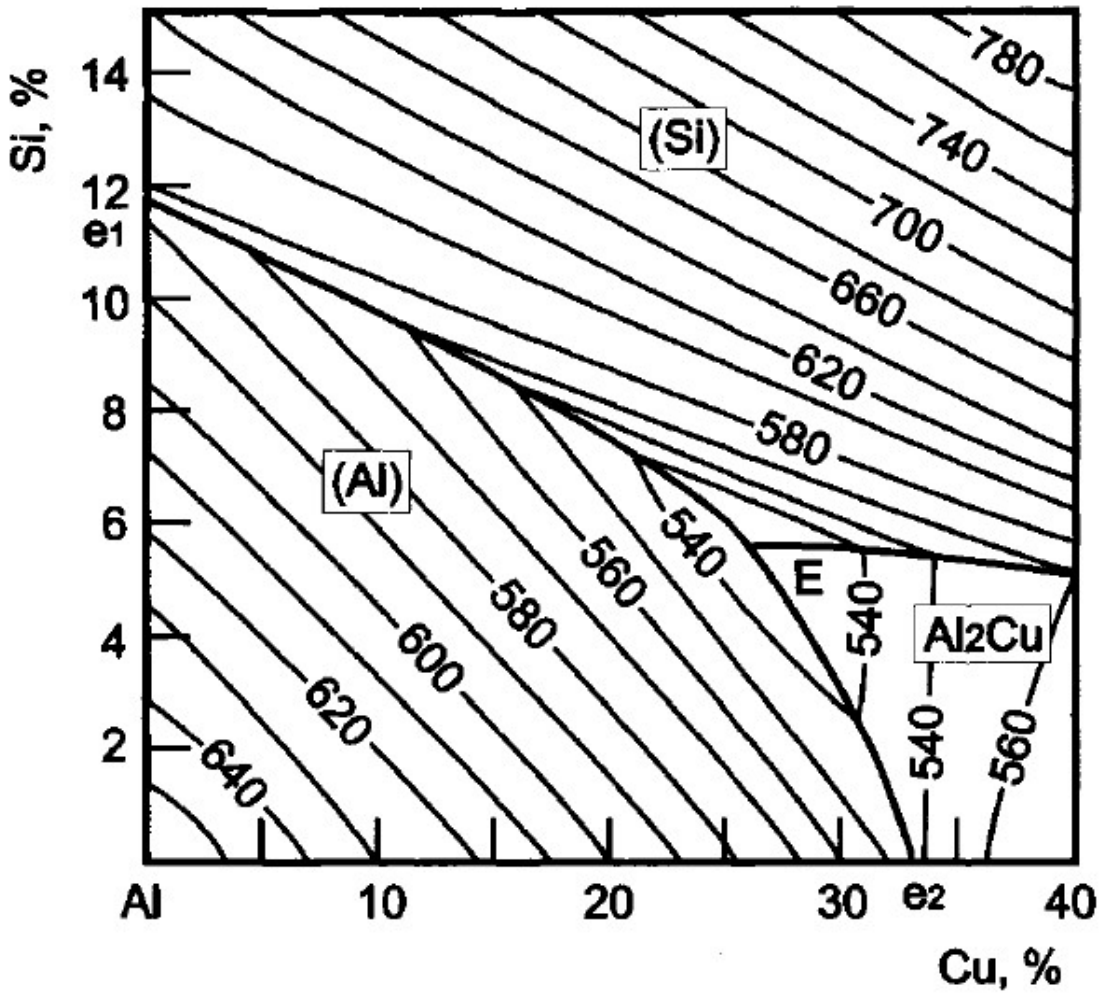

Figure 12 Phase diagram of Al-Cu-Si system (liquidus) [16]

2.3 Refinement of primary Si

2.3.1 Generality

Primary Si in hypereutectic Al-Si alloys is very hard, improving wear resistance of the alloys, but decreasing tool life during machining. Controlling the size, shape and distribution of the primary Si particles in hypereutectic Al-Si alloy castings is commonly known as refinement. It is based on maximizing the number of sites on which primary Si crystals can nucleate.

As said previously, many problems for hypereutectic Al-Si alloys are caused by the coarse primary silicon particles, so a refinement of the particles will make the alloys more useful and more interesting for critical applications. Grain refiners (inoculants) which can act as nucleation sites for primary Si crystals can be introduced during solidification to promote the heterogeneous nucleation. Investigation in order to find effective grain refiners for aluminium grains in different aluminum alloys can be

tracked back to the early 1950s. The attempts have led to introduction of grain refiners (master alloys) such as Al- Ti, Al-Ti-B, Al-Ti-C and Al-B. Phosphorous in the form of pure P and CuP or Al-P master alloys have been proved as effective refiners for primary Si in hypereutectic Al-Si alloys. The refinement of primary silicon crystals was also found with addition of rare earth element [8]. Some examples of grain refinement are shown in fig. 13, comparing the refinement among phosphorus and RE in Al-20Si.

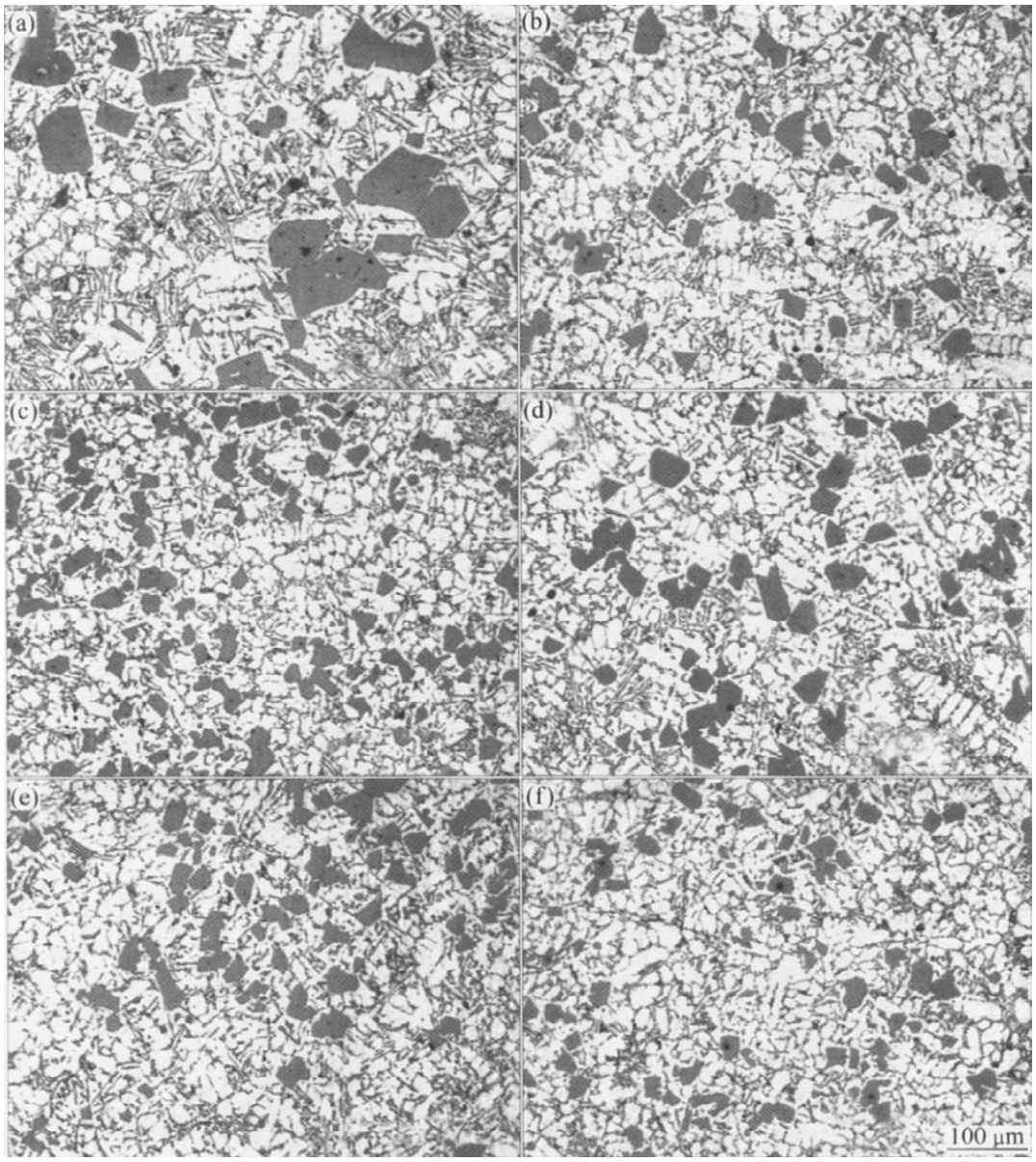

Figure 13 Primary silicon morphologies of Al-20Si alloys modified with different modifiers: (a) P and RE free; (b) 0.06% P and 0.6% RE; (c) 0.08% P and 0.6% RE; (d) 0.1% P and 0.6% RE; (e) 0.08% P and 0.3% RE; *(0* 0.08% P and 0.9% RE). [8]

The effect is similar using other master alloys (fig.14) [9].

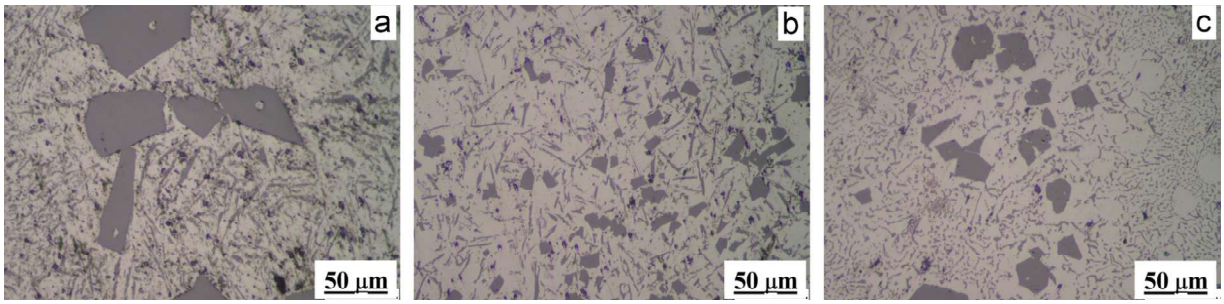

Figure 14 Microstructure of the alloy Al–18Siunmodified (a),modified with master alloy Al–8Fe–2P (b)and modified with master alloy Al–10Sr–1P (c)states(LM). [9]

2.3.2 Al-3P master alloy

Among different chemical modifiers, P is widely used to refine the primary Si particles because the AlP formed in the melt can act as the heterogeneous nucleation sites for primary Si. In general Hypereutectic alloys have shown fast refinement response to the addition of Al−P master alloys. After refined at 780℃ for30 min, the coarse primary Si in Al20Si alloy can be refined from 90 μm to less than 20 μm. In addition, the morphologies of primary Si are changed from coarse polygon to near-sphere shape, and the distribution is improved simultaneously [10]. This is a good point as regards the mechanical properties because coarse polygon and platelet cause the serious disseverance to the matrix. Fig.15 shows how the particles of the master alloy work as the nucleation point for the silicon.

Therefore, the solidification process of Al−Si after the addition of Al−3P and master alloys can be described as follows. After adding it into the Al−Si melt, the pre-formed AlP particles gradually start to dissolve ($AlP_{[s]} \rightarrow Al_{[l]} + P_{[l]}$) until the melt is saturated in phosphorus. Due to the lower solubility of phosphorus and the density difference, some AlP particles cannot distribute uniformly in the melt. These undissolved AlP would become the dregs and float to the melt surface, which means that they cannot act as the heterogeneous nucleation sites of primary Si. Since the solubility of P in the melt decreases with the temperature, the P dissolved homogeneously in the melt would precipitate as AlP with decreasing melt temperature, which provide the nucleation sites for primary Si. [9]

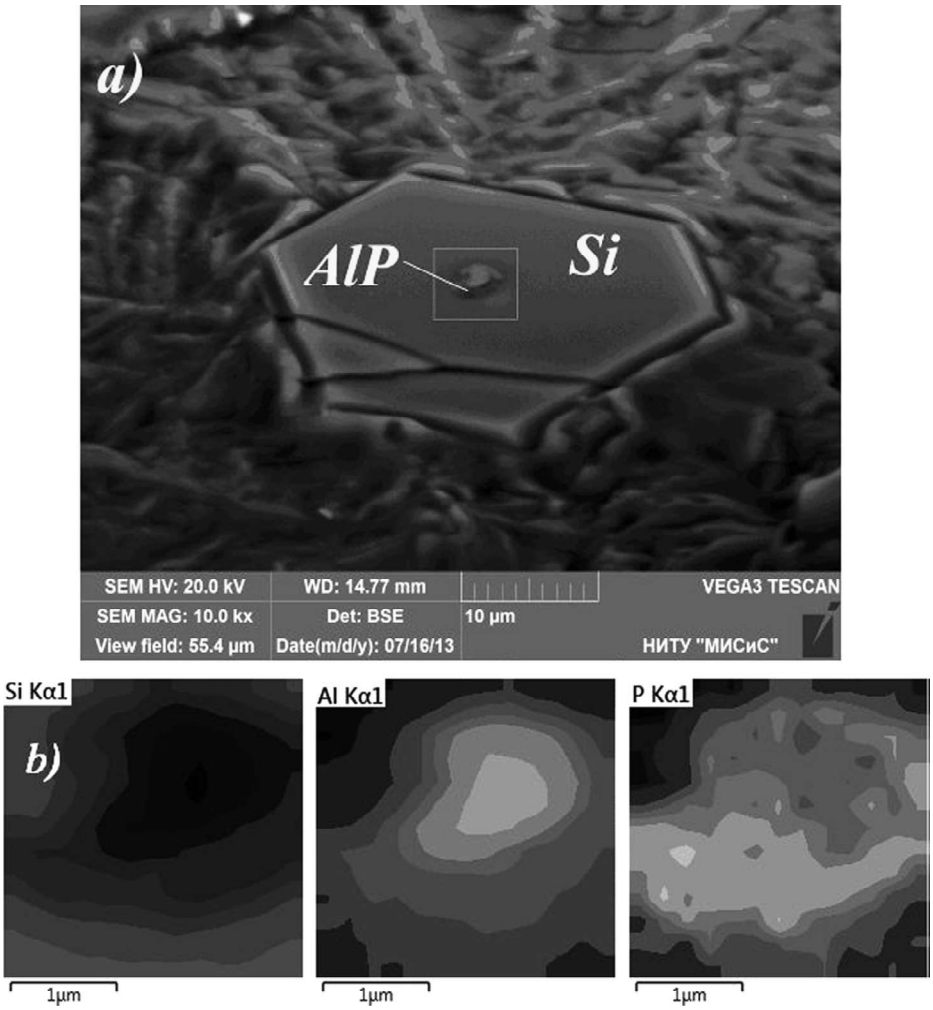

Figure 15 Microstructure of alloy Al–18Si–0.1Sr–0.01P (a) and image of characteristic emission Al, Si and P(b)(SEM). [9]

Aluminum phosphate (AlP) particles are commonly accepted to be the nucleation site (fig.15) for primary silicon hypereutectic Al-Si alloys, since both have similar crystal structures as shown in fig.16, and the lattice parameters of Si and AlP are very close with a lattice mismatch of less than 1% .

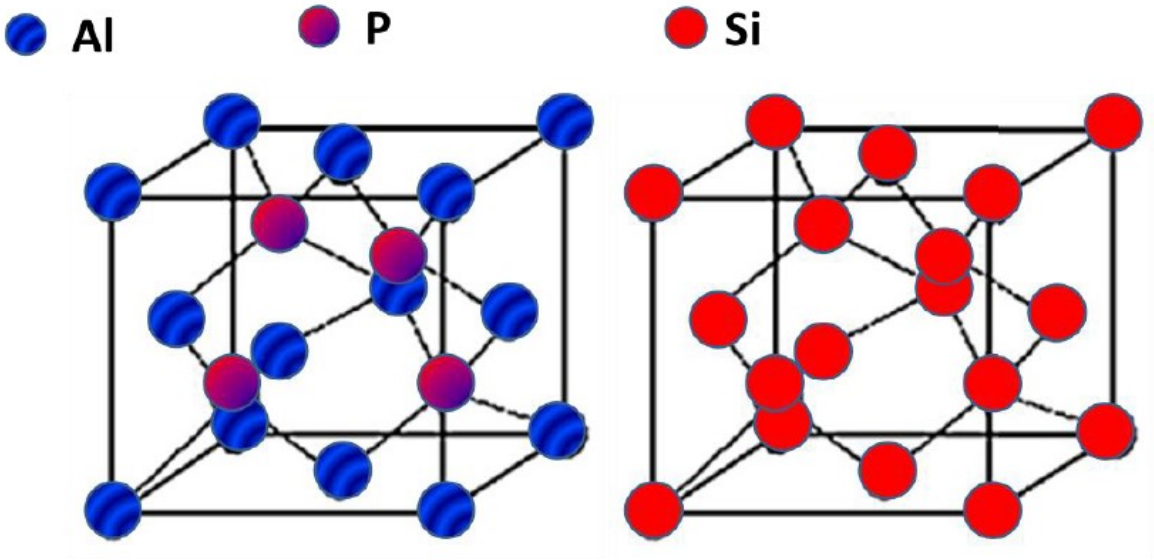

Figure 16 The crystal structures of AlP and Si.[9]

The primary Si nucleates and then grows by wrapping around the AlP nucleant to develop as a compact particle. The compound AlP may also be a common nucleus for eutectic Si in unmodified alloys, but becomes less active in the presence of the modifying element, e.g. Na, or Sr. The mechanism for this transition is unclear but may relate to the reaction of P with intermetallics formed between the modifying element and Al, Mg and Si. Thus an excess of P will lead to refinement of primary Si but little or no eutectic modification, and an excess of Sr will lead to eutectic modification without substantial refinement of primary Si.

2.3 X-ray technique (Micro focus X-ray radiography)

Better understanding of solidification and casting processes of metals is still of high importance, both from a scientific point of view and for industrial applications. X-ray microscopy is a powerful method for investigating the interior of otherwise opaque objects, such as metallic alloys. With the large penetration depth of x rays, dynamic processes—such as solidification—can be investigated in the bulk, giving direct insight into the opaque material without affecting the process. Recent developments of new and powerful synchrotron radiation sources, optics, and detectors allow for in situ investigation of solidification processes. Compared to synchrotron radiation sources, contemporary micro focus tubes generate x-rays with lower but still substantial brilliance. At the same time their power requirements are quite modest. Figure 17 shows the micro focus X-ray system.

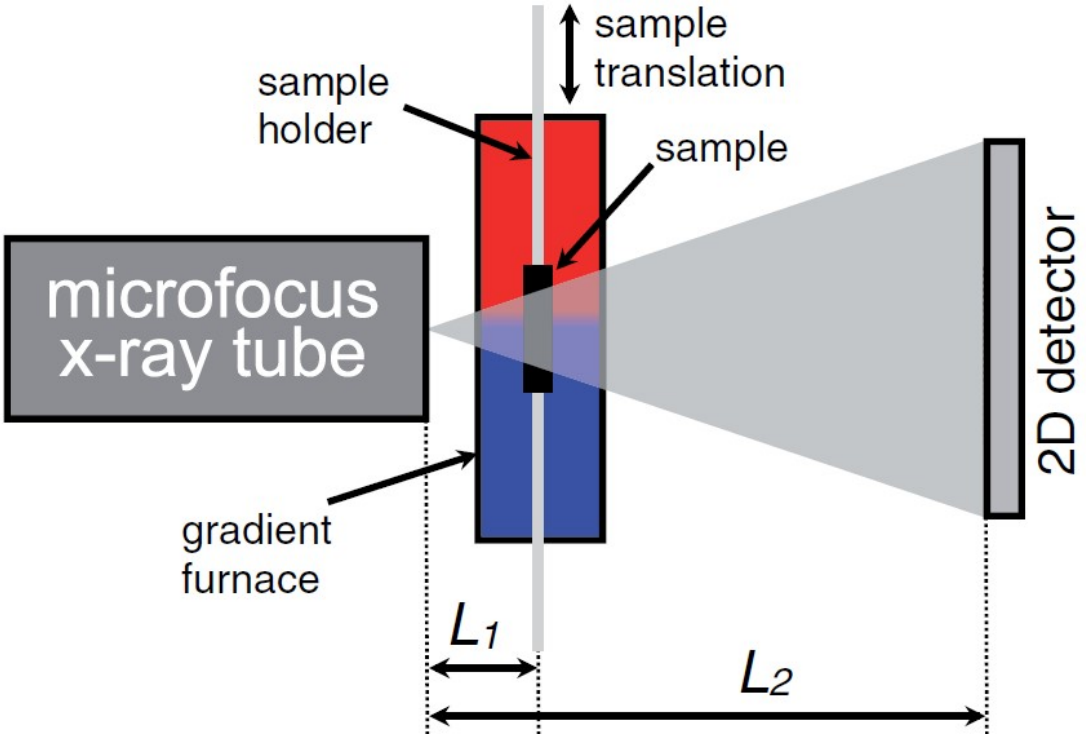

Figure 17 Schematic device setup [18]

The smaller the source size, the smaller is the blurring of the image on the detector and also the higher is the spatial resolution. In addition, the more photons are emitted into the solid angle subtended by the detector, the shorter is the exposure time.[18]

The detector is usually a sheet of photographic film, held in a light-tight envelope or cassette having a very thin front surface that allows the X-rays to pass through easily. Chemicals are needed to develop the image on film, which is why this process is called the classic or " wet" process.

The source of radiation should be physically small (a few millimeters in diameter), and as X-rays travel in straight lines from the source through the specimen to the film, a sharp "image" is formed of the specimen and discontinuities. This geometric image formation is identical to the shadow image with a visible light source. The sharpness of the image depends, in the same way, on the radiation source diameter and its distance away from the surface on which the image is formed.

The "classic" film in its light-tight cassette (plastic or paper) is usually placed close behind
the specimen and the X-rays are switched on for an appropriate time (the exposure time) after which the film is taken away and processed photographically, i.e. developed, fixed, washed and dried. In direct radiography (DR), a coherent image is formed directly by means of an computerised developing station. The two methods have a negative image in common. Areas where less material (less absorption) allows

more X-rays to be transmitted to the film or detector will cause increased density. Although there is a difference how the images are formed, the interpretation of the images can be done in exactly the same way. As a result, the DR- technique is readily accepted.

The quality of the image on the film can be assessed by three factors, namely :

- Contrast
- Sharpness
- Graininess

In this work, the first aim was increase the contrast during the x-ray analysis so as well-mark the primary silicon particles during the growth process.[17]

4 Experimental

4.1 Casting

In this part of the work the cooling curves for the solidification of different alloys were analyzed in order to characterize the phase transformations from liquid phase to solid phase, passing through the precipitation of primary silicon phase .

First of all the thermocouples had to be calibrated in the pure aluminum. The process followed was: measurement of the liquidus temperature of pure aluminum by the new thermocouples during solidification. The temperature is recorded by a data-logger. Solidification cycles have to repeated until the reading temperature of the liquidus is constant from cycle to cycle. By this the thermocouple can be stabilized around 6-7 solidification cycles might be necessary, depending on the thermocouple. The accuracy of the thermocouple can be evaluated by comparing the reading liquidus temperature with the known liquidus temperature of pure aluminum.

For the latter purpose pure aluminum (99%) was used whereas the melting point is well-known and it is 660,32 °C.

The experimental Al-20Cu-18Si alloy was prepared by using commercial purity Al, high purity Al, solar grade Si and pure Cu. Al-3P master alloy was used to add P in the alloys. In the first round, four different alloys were cast with different addition levels of phosphorus: 0 p.p.m, 60 p.p.m., 100 p.p.m and 150 p.p.m. In the second round, one alloy with addition of 200 p.p.m P and another two alloys with addition of 150 p.p.m P were cast with different superheating temperature. Table 2 shows the alloys and the addition level of P.

Table 2 Amount of Al,Si,Cu,AL3p

	Al [g]	Si [g]	Cu [g]	Al3P [g]	Total [g]
1° Alloy (0ppm)	620,32	180,02	200,11	0	1000,45
2° Alloy (60ppm)	632,66	183,66	204,08	2,04	1022,44
3° Alloy (100 ppm)	637,73	184,96	205,72	3,42	1031,835
4° Alloy (150 ppm)	645,80	187,49	208,32	5,21	1046,82
5° Alloy (150ppm)	777,14	225,62	250,69	6,27	1259,71
6° Alloy (200ppm)	754,53	219,06	243,40	8,11	1225,10

All of these amounts respect the main percentage of **62% Al, 20 % Cu, 18% Si,** with different levels of master alloy**.** The preparation of the amounts was made by cutting machine for Al, Si and Cu while for the master alloys we used a more precise machine due to the low amounts to be weighed.

The next step was to melt the alloy with the detailed procedure as follows:

- Start the ovens (fig.18) with a preset heating temperature that varies from 850 °C and 950 °C depending on which temperature the liquid has to reach;
- Coated the crucible with Boron Nitride spray in order to reduce contamination of aluminum melted by the crucible. Put the crucible inside the oven with only the aluminum and wait around thirty minutes until Al metal are completely melted;
- Remove the oxide on the top and add copper, wait just a couple of minutes and then stir the melt to get Cu dissolve homogeneously in Al melt.
- Add the silicon and wait until the Si crystal is fully dissolved;
- At the desired temperature, Al-P master alloy was added into the melt and keep the melt at the temperature for thirty minutes to make sure the master alloy was completely dissolved in the melt;
- After removing the oxide film, degassing by pure argon for 8 minutes was applied.

Figure 18 imagine of the oven used for the casting experiments

This degassing step is quite important for reducing porosity in the casting, which it might be a big problem during the later in-situ x-ray radiographic study. The first 4 alloys were cast from the same temperature (800 °C) , the alloy with addition 150 ppm P was cast form 800, 850 and 900°C, and the alloy with addition of 200 ppm P was cast from 900°C. The reasons for this sequence will be explained in the next chapters.

Small graphite crucibles as shown in Fig. 19 were used for cooling curve measurement. Before the casting, the crucibles were pre-heated using anther oven.

Figure 19 Small graphite crucible (scale bar in mm) used for the thermal analyses.

The measurement system consisted of the thermocouple, data logger (fig.20) and PC.

Figure 20 CR23X MICROLOGGER

After it was pre-heated for 4 minutes at 800 °C temperature, the small graphite crucible was filled with the alloy melt and then put on the table and the temperature recording was started. The temperature of the liquid metal were collected by putting the thermocouple in the centre of the crucible. The same location of the sample where the thermocouple was positioned will be analyzed during the light microscope and SEM analysis. In this local position **the cooling rate was measured as 1.1 K/s** and it is almost the same for all the alloys. Three cooling curves were measured for the casting of each alloy so as to make sure that representative cooling curve can be achieved.

After the cooling curve measurements, the rest of the liquid metal was poured into a large copper crucible for preparation of samples for in-situ X-ray radiographic study. The operation is shown in fig.21.

Figure 21 Pouring out of the remaining alloy in a Cu mould

Afterwards other two castings experiments were done using high purity aluminum and copper instead of commercial pure ones. This point will be explained well in the results section, but it was done in order to avoid the phosphorus and other nucleation sites that might be brought by the impurities of commercial purity aluminum and copper, and also to create a new reference alloys for revealing the influence of impurities. The table 3 with the amounts of these high pure raw materials is shown in the following table:

Table 3 Amounts of high pure raw materials

	Al [g]	Si [g]	Cu [g]	Al3P [g]
Reference alloy (0ppm)	437,11	126,90	141,00	/
7° alloy (150 ppm)	429,50	124,69	138,45	3,46

4.2 Preparation of the samples

The samples from the crucible (fig.11) are not directly suitable for analysis with the microscope, so they require some preparation step.

Starting with a normal machine cutting, some cube-shaped samples were obtained. Then the samples were grounded and polished to get metallographic samples. The detailed procedures were as follows:

- The flat surface of the sample was grounded by different grid sand papers: 320, 500, 800, 1200,2400;
- During polishing, diamond paste of with different size of particles 6µm, 3µm and 1µm were used ;

Samples were also prepared for in-situ x – ray radiographic imaging which requires a special kind of samples. First of all, from the alloys casted in the big mold was cut into a parallelepiped (one for each alloy), where afterwards some slices were cut, as shown in fig.22. [7]

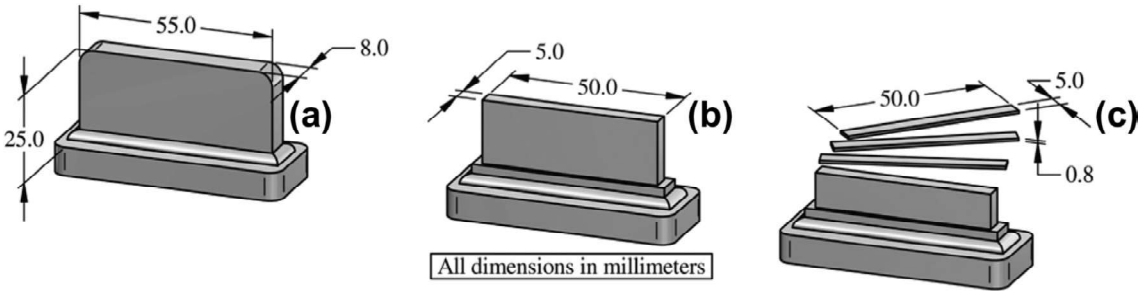

- Figure 22 Dimensions of the samples for x-ray

Then, once the slices with thickness around 1 mm were cut, mechanical grinding was applied to reduce the sample thickness down to 200 µm. A final polishing with 3 µm diamond paste was also done on both sides of the thin foil type samples. Four samples for each alloy were prepared. The image of the final X-ray imaging sample is shown in Fig.23.

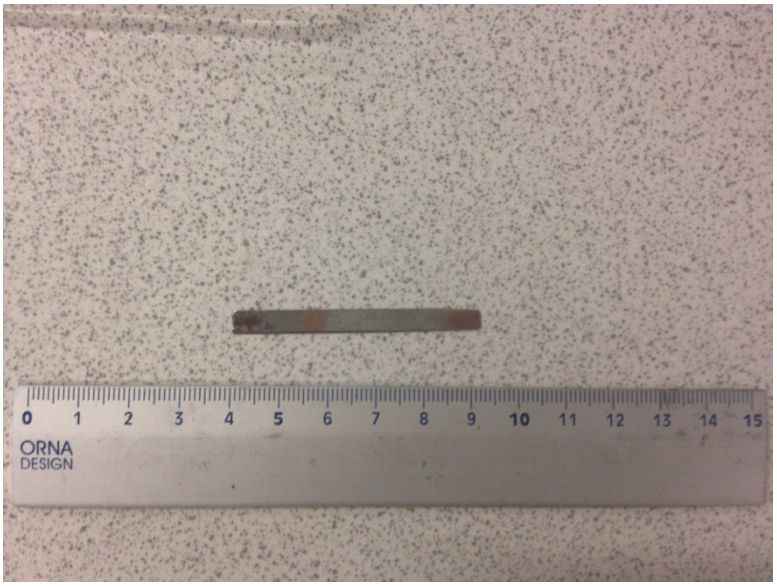

Figure 23 Sample for X-ray analysis (scale bar in mm)

4.3 Chemical analysis

In order to validate the composition of the alloy, in particular the P content, chemical analyses were performed. The technique used is Glow Discharge Mass Spectrometry (GDMS), because it has very good detection limits (required for P). GDMS employs discharge sputtering. The sample atoms are ionized by interactions with the metastable sputtering gas (generally argon). In GDMS the resultant ions exit from the high-pressure region through an orifice into a higher vacuum (10-5 to 10-6 torr) where they are mass analyzed, typically by a quadrupole mass filter. Full mass scans permit qualitative and quantitative analysis . As sputtering exposes successively deeper layers, repetitive monitoring of one or more masses facilitates depth-profiling analysis [15]. The GDMS used in this study is well calibrated for P, however for copper and silicon the data are not accurate.

4.4 Light microscope

The first investigation is made by light microscope. A “Leica DMi8 for Industry” (fig.24) was used. Digital images were taken.

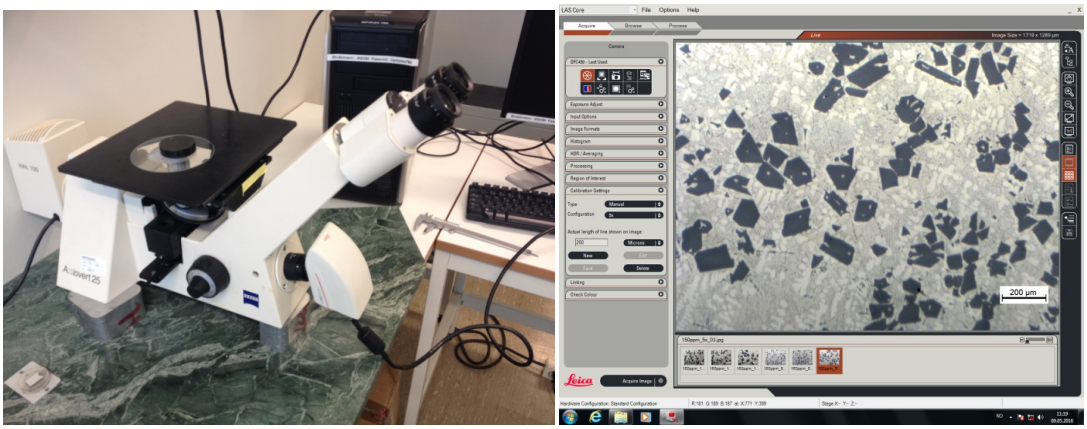

Figure 24 Microscope and software used

Afterwards these pictures were analyzed with an image analysis software, “ImageJ”. The size and number density of primary Si were measured after some image processing steps, including calibration of the scale bar, giving the length of each pixels and generation of binary image by setting optimum threshold values to separate the Si particles from the matrix. An example for the image processing is shown in Fig. 25.

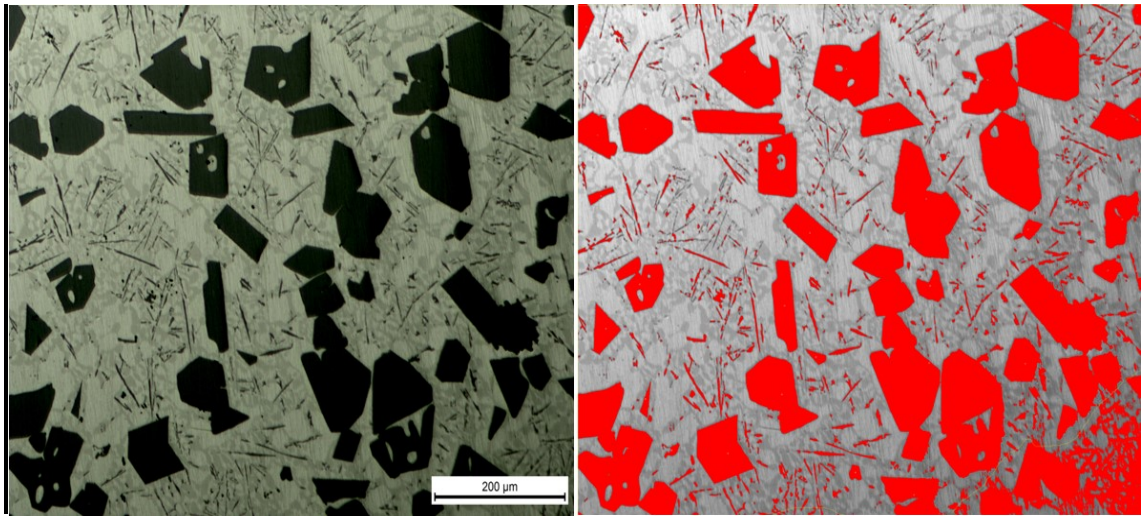

Figure 25 The first image is without thresholding and the second after thresholding

With the binary image, the software is able to count the number and size of Si particles automatically, giving the number density and average size (equivalent diameter).

4.5 In-situ X-ray radiographic study

In order to study the nucleation and growth of primary silicon during solidification of hypereutectic Al-Si alloys the micro focus X-ray radiography instrument was used. The solidification process was studied in-situ. In particular this instrument is composed of different parts:

- First of all there is a x-ray generator made by an electron cannon which impacts with a Mo target which emits x-ray;
- A Bridgman furnace (fig.27) was used to melt the foil type sample and have the solidification proceed under different cooling rates and temperature gradients.;
- The x-ray pass through the sample and they hit a detector which can transform the x-ray signal in a visible pictures;
- The temperature is continually checked by two thermocouples, one in the top of the sample and one in the bottom;

The schematic diagram can show better how the instrument works (fig.26).

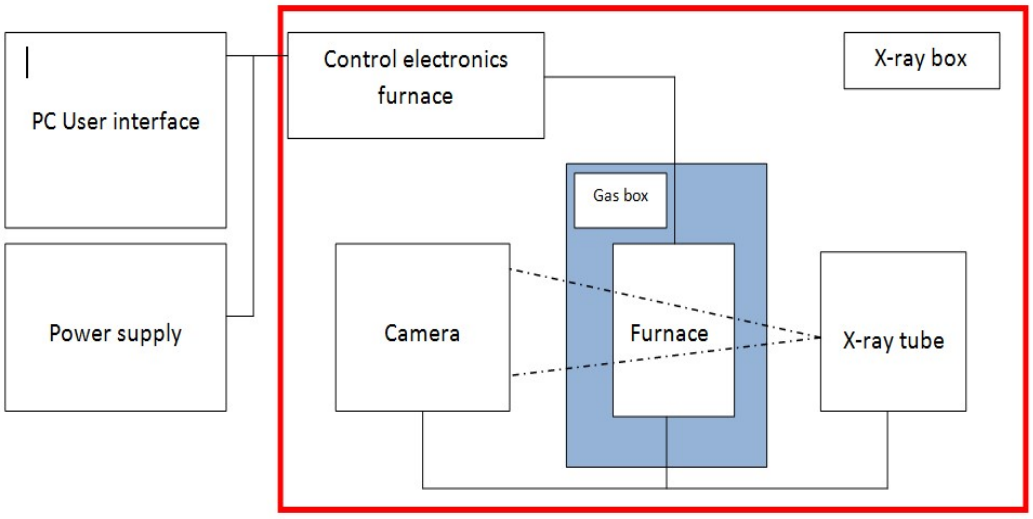

Figure 26 Block diagram of X-ray machine

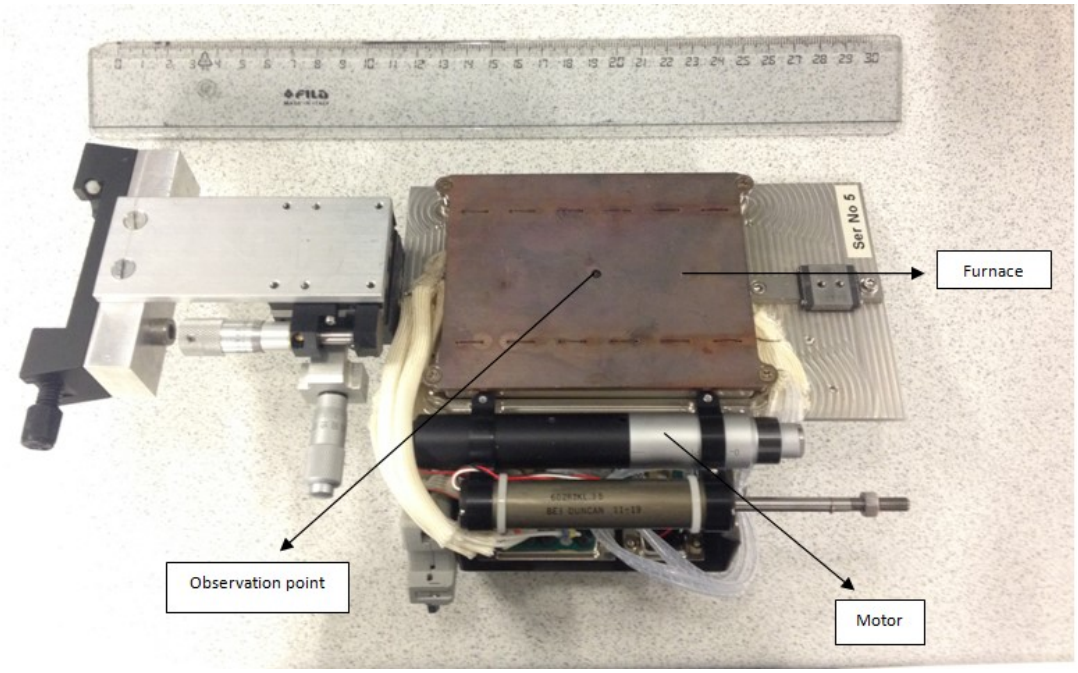

Figure 27 The furnace

The complete machine is shown in fig.28 :

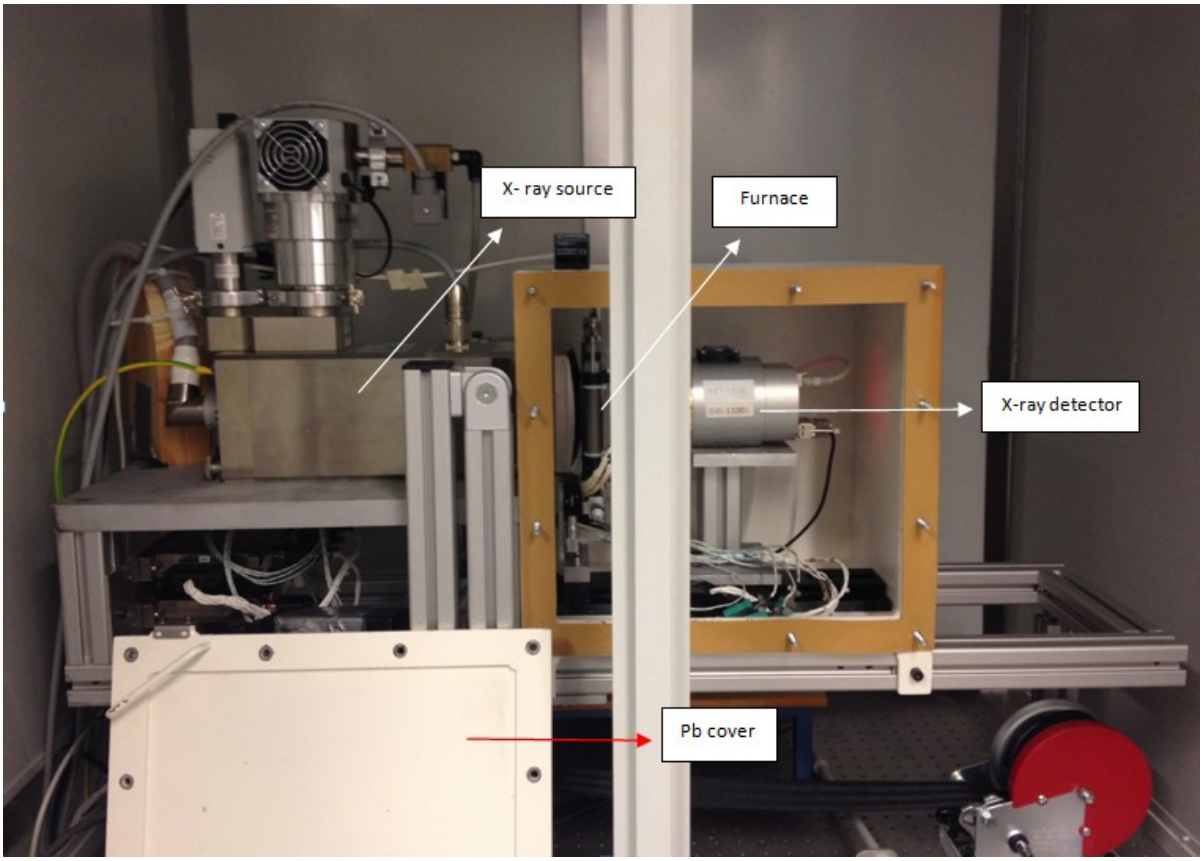

Figure 28 X-ray machine

First of all the sample was put inside the sample holder; the sample is held by a metallic support and sealed by two thin glass carbon films which are transparent for the x-ray. The equipment is shown in fig.29.

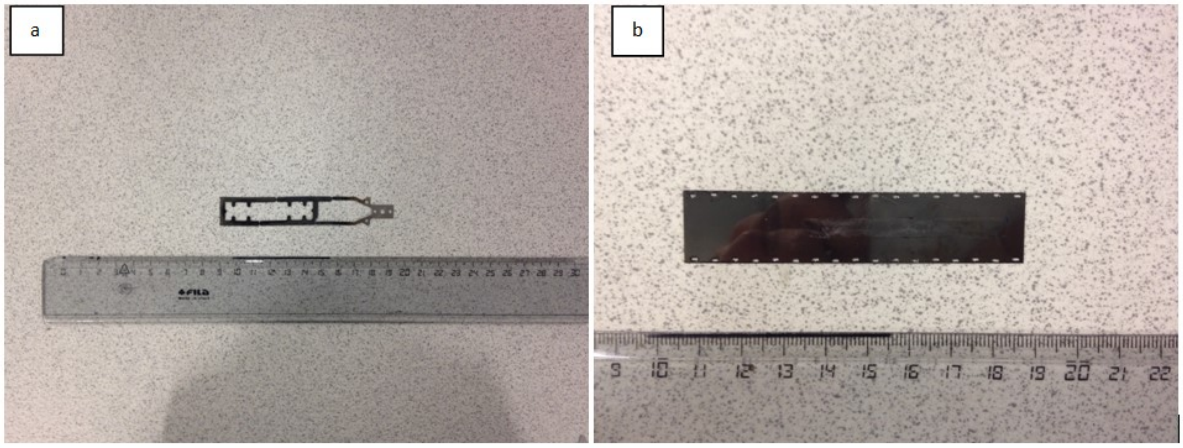

Figure 29 a) the metallic support and b) the carbon glass used for the X-ray radiography (scale bar in mm)

Afterwards the sample holder was put inside the bridgman furnace and where two thermocouples cables were fixed. Then some attempts were done so as to find the best spot to film. In fact, as said previously, the experimental cast alloys have always some porosities even if, a long time of degassing was done, before casting. In order to avoid the oxidizing of the samples during melting and solidification in the bridgman furnace, pure nitrogen was filled in the box to reduce the oxygen concentration down to 1%. All the experiments were conducted by heating the samples up to the limit of the furnace (800 °C) and then this temperature was kept as long as the primary silicon was completely melt, checking thanks to the computer video. The melting and solidification of the foil type was done in the horizontal position by putting the x-ray source above, while the detector was put below the sample broad surface. Such an arrangement will greatly reduce the convection and floating of primary Si crystal caused by density difference between different phases in the melt.

The cooling rate was set from the PC, with different values: **0.1 K/s, 0.025 K/s, 0.5 K/s, 1.2 K/s.** The maximum cooling rate for the instrument is 2 K/s, but according to the previous experiments the maximum cooling rate needed was 1.2 K/s. All the cooling cycles with different cooling rates were done twice and then the best and the clearest will be selected. The acquisition rate was set as: 1 Hz for 0.1 K/s, 0.025 K/s, 0.5 K/s and 2 Hz for 1.2 K/s. Once the primary silicon was completely melted, a flat filed was taken as a reference image for later image processing to improve the contrast of images of the recording video. The cooling and imaging were stopped as soon as the primary particles reached the final number density and shape at around 700 °C, before the eutectic point. One cooling cycle was continued until the eutectic point was reached,

where the eutectic temperature was used to calibrate the real temperature in the melt of the sample. The different stages during the solidification are shown in fig.30.

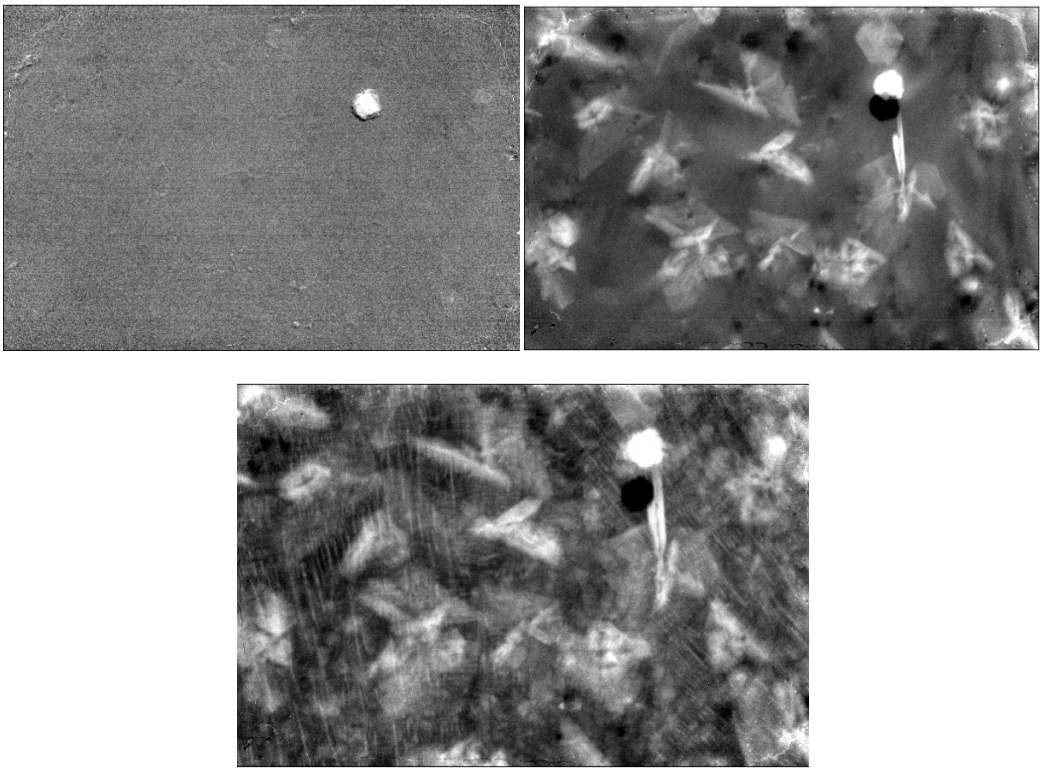

Figure 30 From right to left: liquid stage, primary silicon particles, primary silicon with eutectic phase

In order to see and understand the floating phenomenon some vertical and diagonal experiments were done. The aim was to catch the vertical motions of the particles during the solidification stage. The cooling rate was set as 0.5 K/s. Moreover the bottom part of the furnace was set with a lower temperature so as to increase the floating .

5 Results and discussion

5.1 Cooling curves and liquidus temperatures

As it has been said, during every casting, inside the small crucible, a thermocouple was inserted to measure the cooling rate and the nucleation. The results are shown in the following graphs.

5.1.1 Alloy prepared by commercial pure Al alloys

The first group of alloys was prepared by using commercial purity raw metals. The cooling curves for the solidification of Al-20Cu-18Si alloys with different addition levels of phosphorus, are shown in figures 31,32,33,34.

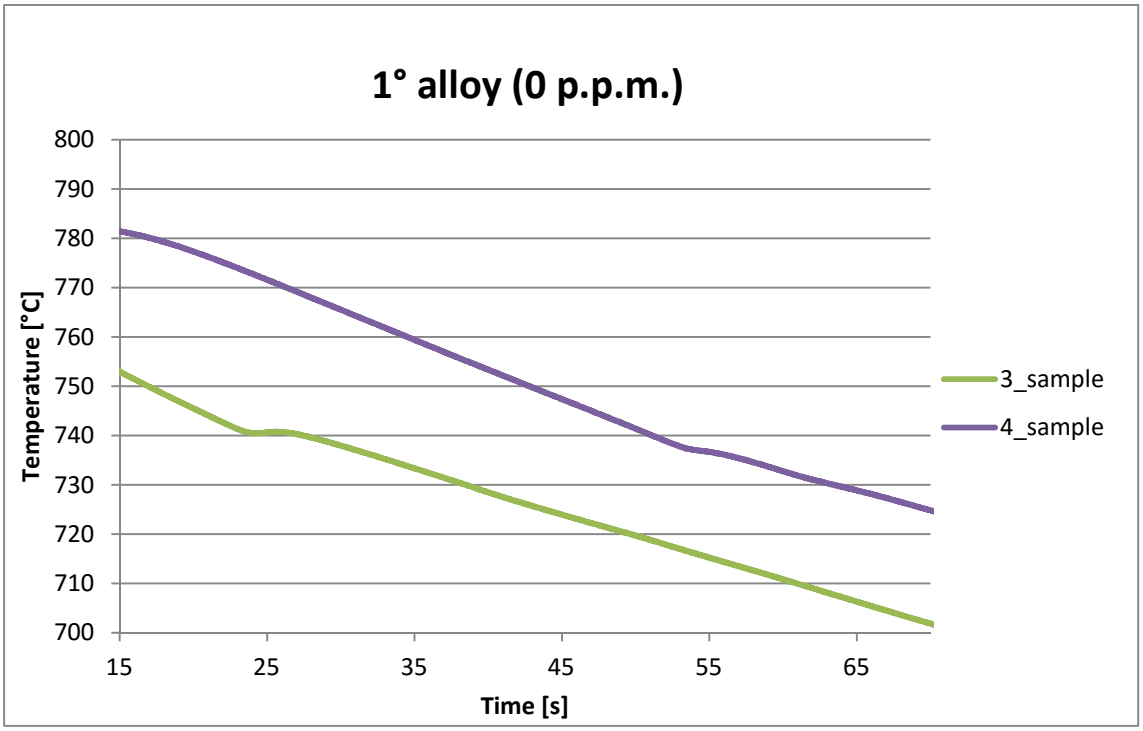

Figure 31 Cooling curve of 1° alloy

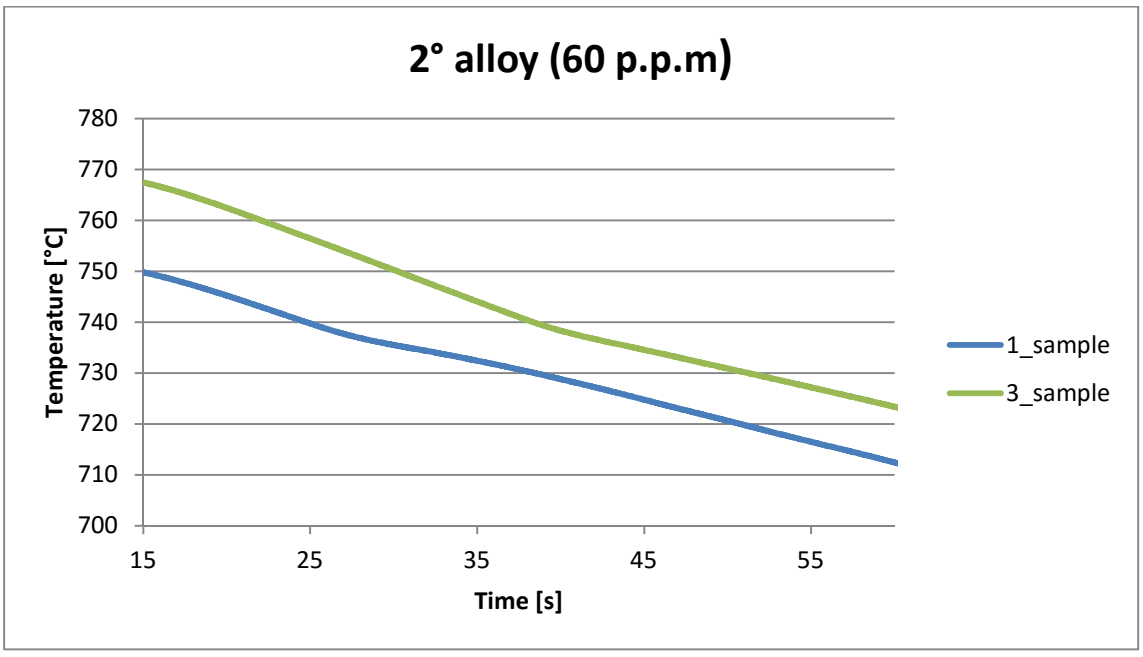

Figure 32 Cooling curve of 2° alloy

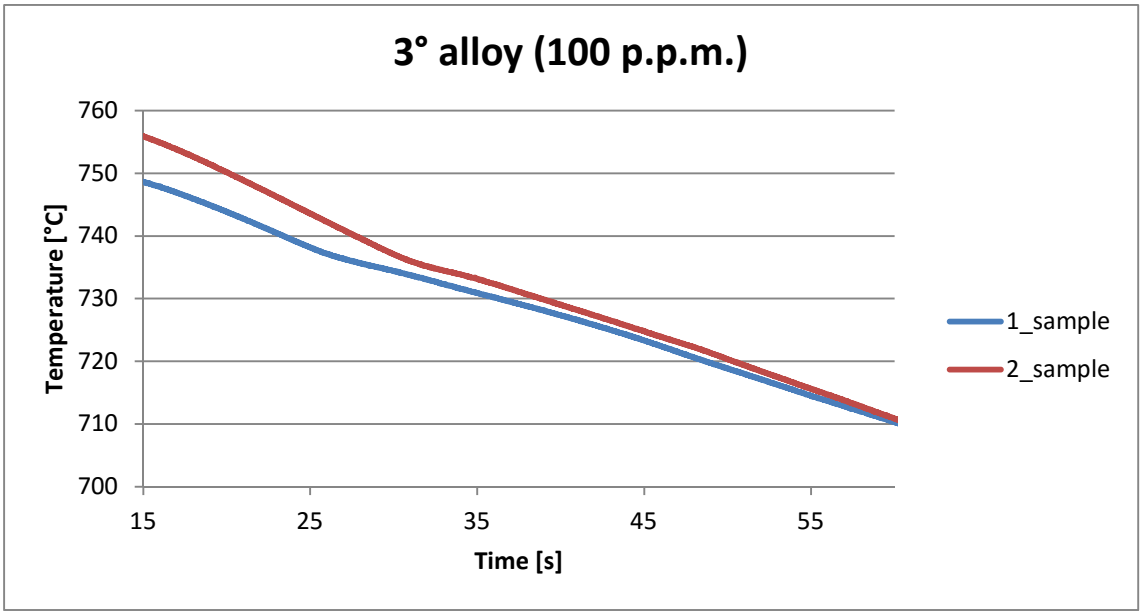

Figure 33 Cooling curve of 3° alloy

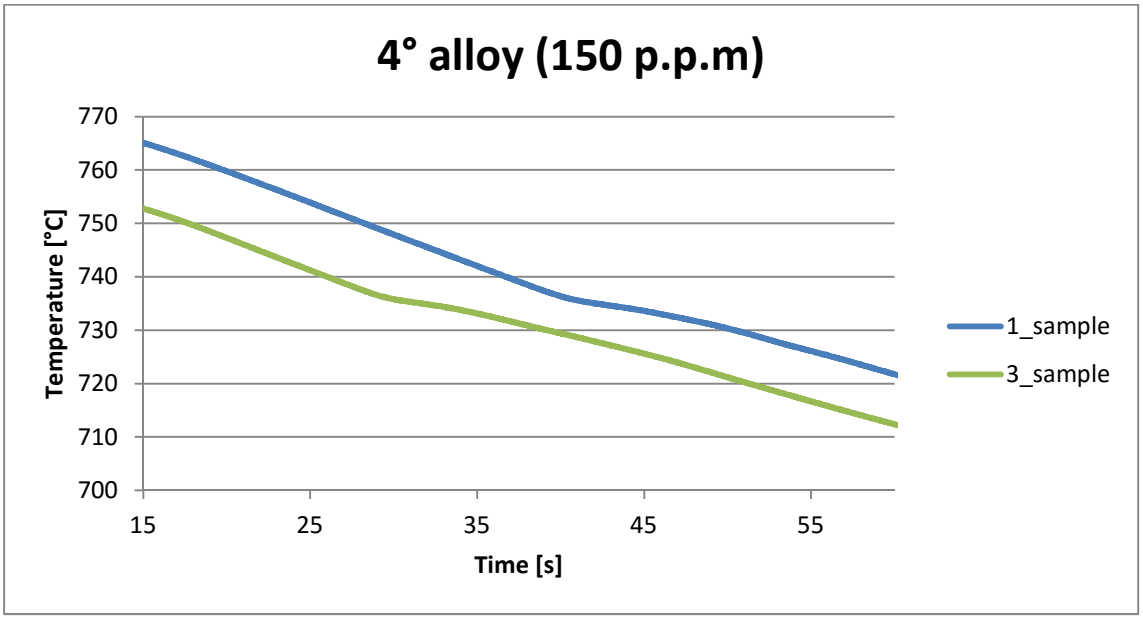

Figure 34 Cooling curve of 4° alloy

The analysis was stopped after this level because of the similarity of the curves, but anyway some good considerations were got:

- There is a clear flat part in every curve;
- This stage is within a small range of temperature;
- The cooling rate is 1,2 K/s.

For this last reason, after a first derivative analysis, the nucleation temperatures were collected, and they are reported in tab.4.

Table 4 nucleation temperature

	T° start [°C]
1°alloy_0ppm	736.5
2°alloy_60ppm	738
3°alloy_100ppm	737.5
4°alloy_150ppm	737.5

5.1.2 High pure raw material

As it has been seen, for the alloys prepared by using commercial pure raw metals, there was not a big difference on the shape of the curves and on the nucleation temperature of primary Si, so another two alloys prepared by using high purity Al and Cu were cast. They were done only with two levels of phosphorus: 0ppm and 150 ppm. The cooling curves are shown below:

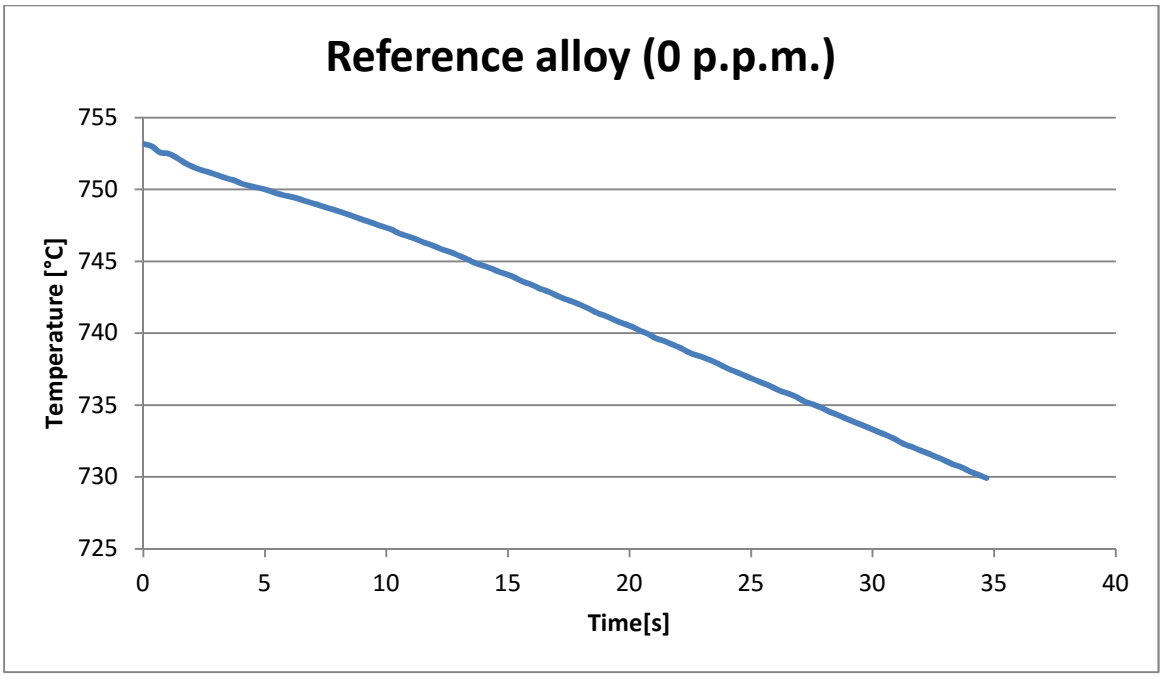

Figure 35 Cooling curve of reference alloy

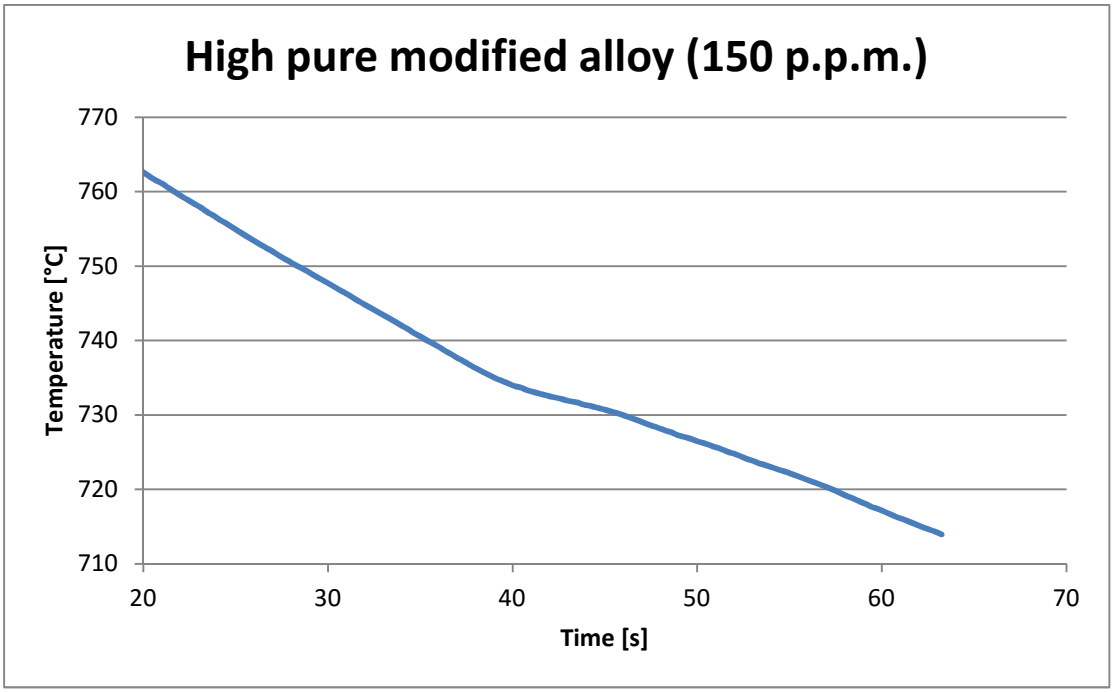

Figure 36 Cooling curve the modified alloy with high pure raw material

In these graphs it is clear that the reference alloy has not the flat part as the casting modified by 150 ppm P. Even with a derivative analysis it was not possible to detect the nucleation temperature of primary Si. The slopes of the curves in the two are about the same, meaning that the cooling rates are the same. From the second cooling curve, the one of the alloys with 150 ppm, there were no differences with the previous alloys as it was expected. Conversely as regards the reference alloys the cooling curve has one important difference: there is no flat part at all. It is in accord with what was expected because if there is less phosphorus or even not phosphorus at all inside the liquid there should be less nucleation points so the particles that start to grow are fewer, and with fewer particles the system takes less energy to solidify; then the cooling stop (the flat part) is not appreciable as in the other alloys with phosphorus.

5.2 Chemical analysis

It is well known that the phosphorus is a volatile element, so in order to validate the value of the amounts supposed, chemical analysis with GDMS technique were done. The measured concentration of P in different alloys are shown in the table 5.

Table 5 Right level of phosphorus in each alloy

Alloy	P [p.p.m]
1st_0ppm	72 ± 2
2nd_60ppm	38 ± 1
3rd_100ppm	109 ± 3
4th_150ppm	74 ± 9
4th_150ppm_900 °C	97 ± 3
5th_200ppm_850 °C	75 ± 5
High pure (reference)_0ppm	0,47 ± 0,01
2nd High pure_150ppm	110 ± 2

The number after the ppm in 4th and 5th alloy represents the casting temperature.

The results of silicon and copper are not reported because this technique is not accurate to catch high concentration of alloying elements in the alloy. The results are different as it was expected, except for the alloy made by using high purity Al and Cu. Therefore, it means that the commercial pure Al and Cu metals may also contain some P as impurities.

The chemical analysis by GDSM shows some differences with the expected values. First of all the amounts of phosphorus were different in all the alloys. This is due to the impurities inside the raw material that can give additional P. Then the amount of silicon and copper was not reported because this tool is set for measuring low amounts of elements.

5.3 Light microscope pictures

5.3.1 Size and shape of the primary silicon particles

The first tool to characterize the phosphorus effects was the light microscope analysis. The pictures that were collected are the following. The first six pictures came from the alloys made of commercial purity raw metals.

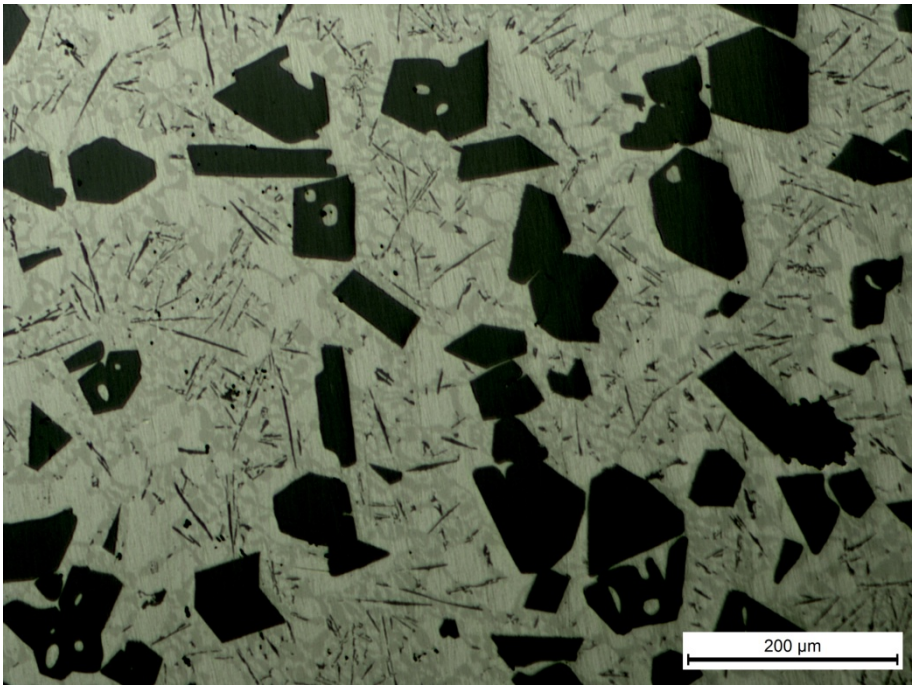

Figure 37 The microstructure of the 1st alloy (0 ppm supposed and 72 ppm real)

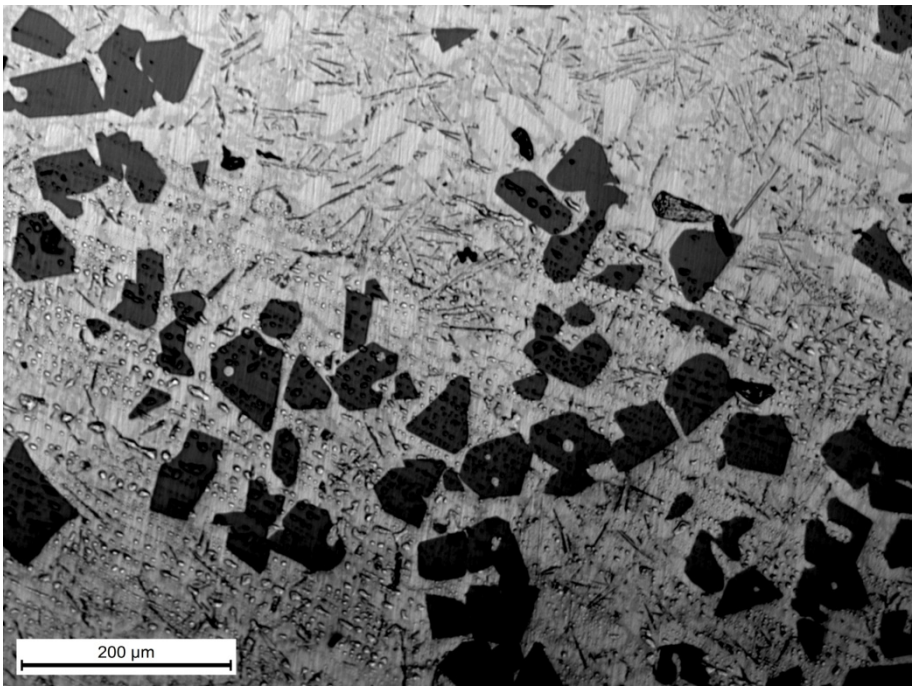

Figure 38 The microstructure of the 2nd alloy (60 ppm supposed and 38 ppm real),

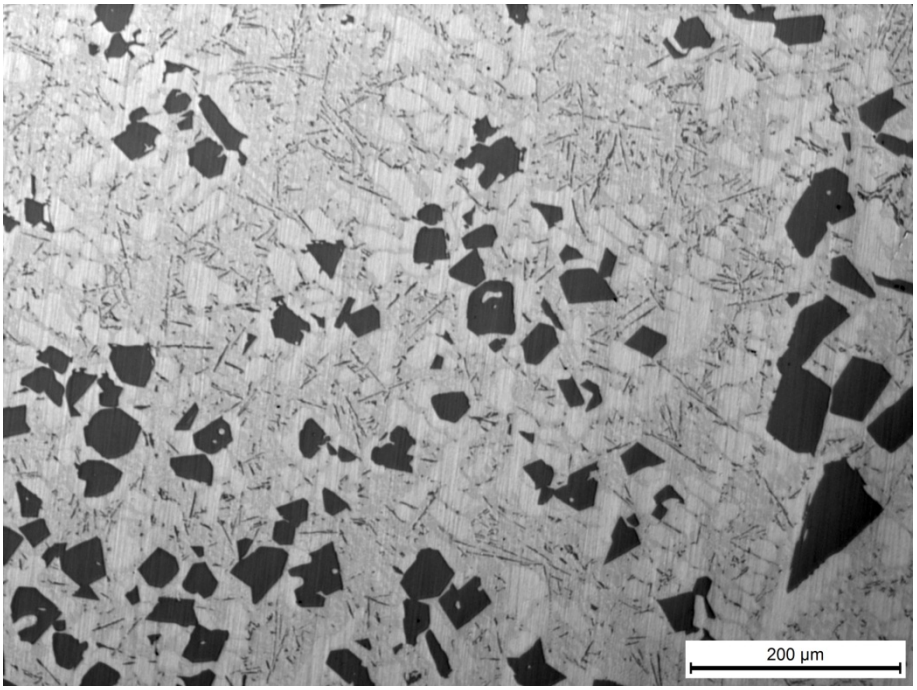

Figure 39 The microstructure of the 3rd alloy (100 ppm supposed and 109 ppm real)

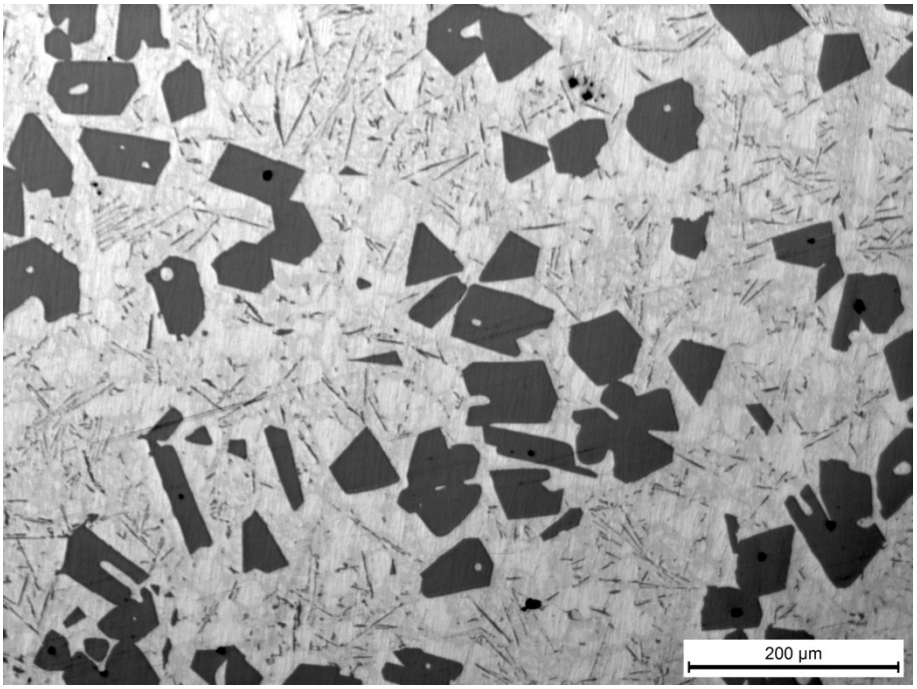

Figure 40 The microstructure of the 4th alloy (150 ppm supposed and 74 ppm real)

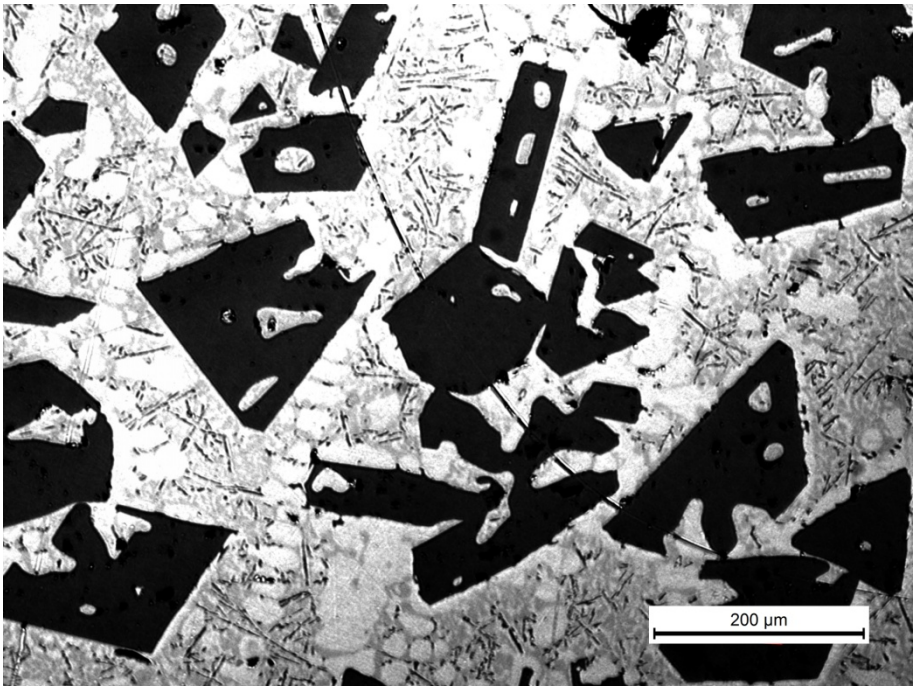

Figure 41 The microstructure of the 4th alloy (150 ppm supposed and 97 ppm real), casted from 900 °C

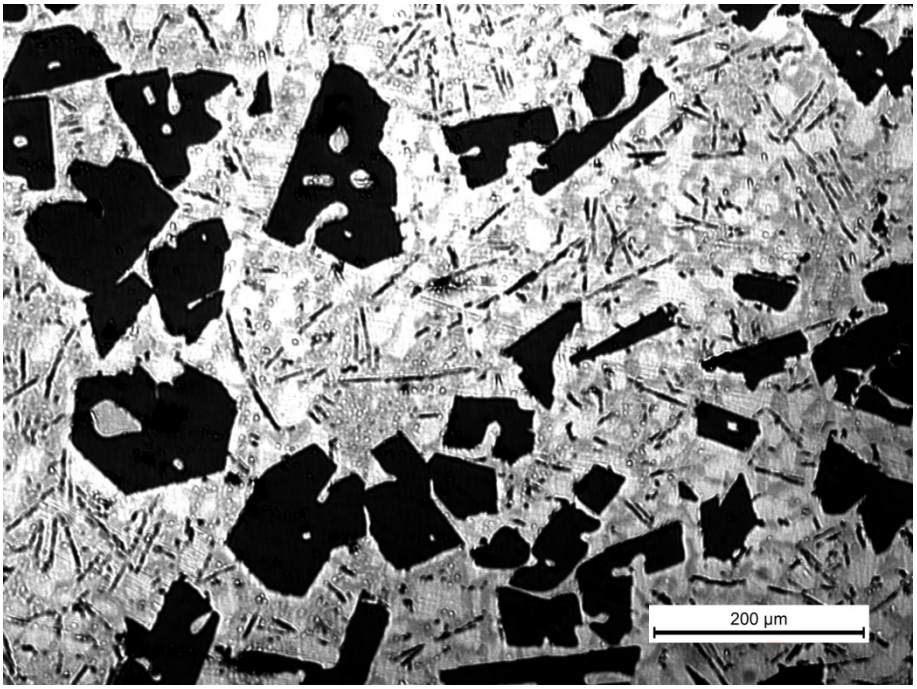

Figure 42 The microstructure of the 5th alloy (200 ppm supposed and 75 ppm real), casted from 850 °C

Then the alloys made of high purity raw metals :

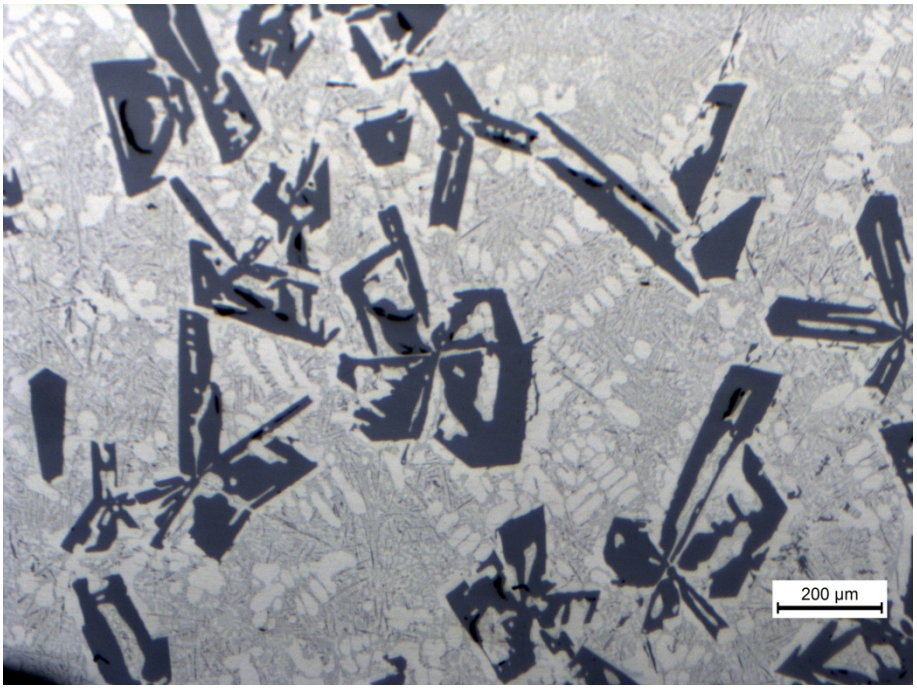

Figure 43 The microstructure of the reference alloy (0 ppm supposed and 0 ppm real)

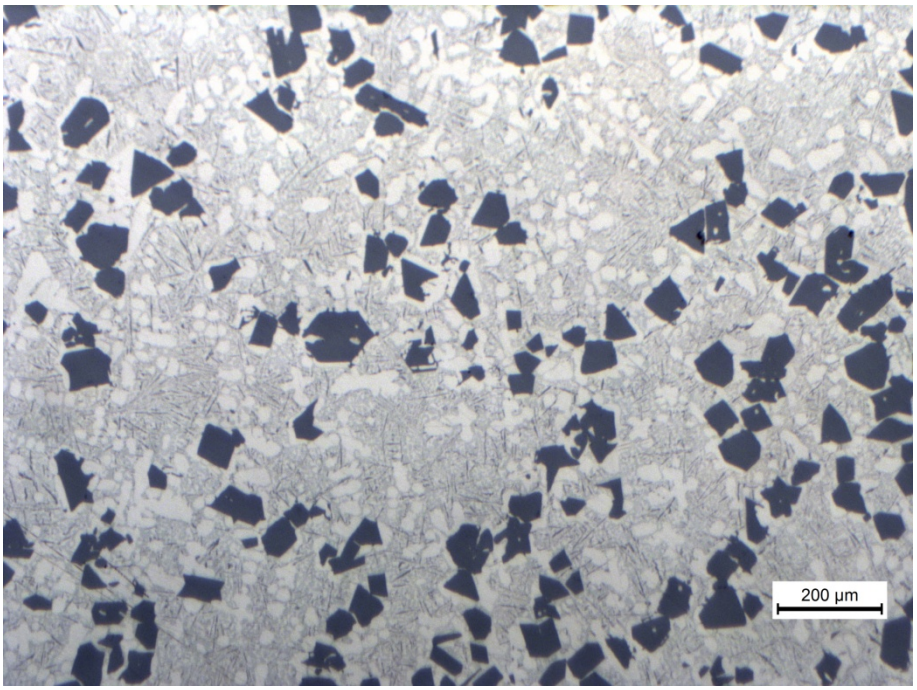

Figure 44 The microstructure of the 2nd high pure alloy (150 ppm supposed and 110 ppm real)

The average size of primary Si particles were measured by using ImageJ software, the results are shown in the following chart. As a general trend, the size of primary Si

particles decreases with increasing adding level of P in the alloys. If comparing the alloys prepared by using high purity metals and commercial purity metals, we can see that at the same P addition level , the latter alloys have smaller primary Si particles.

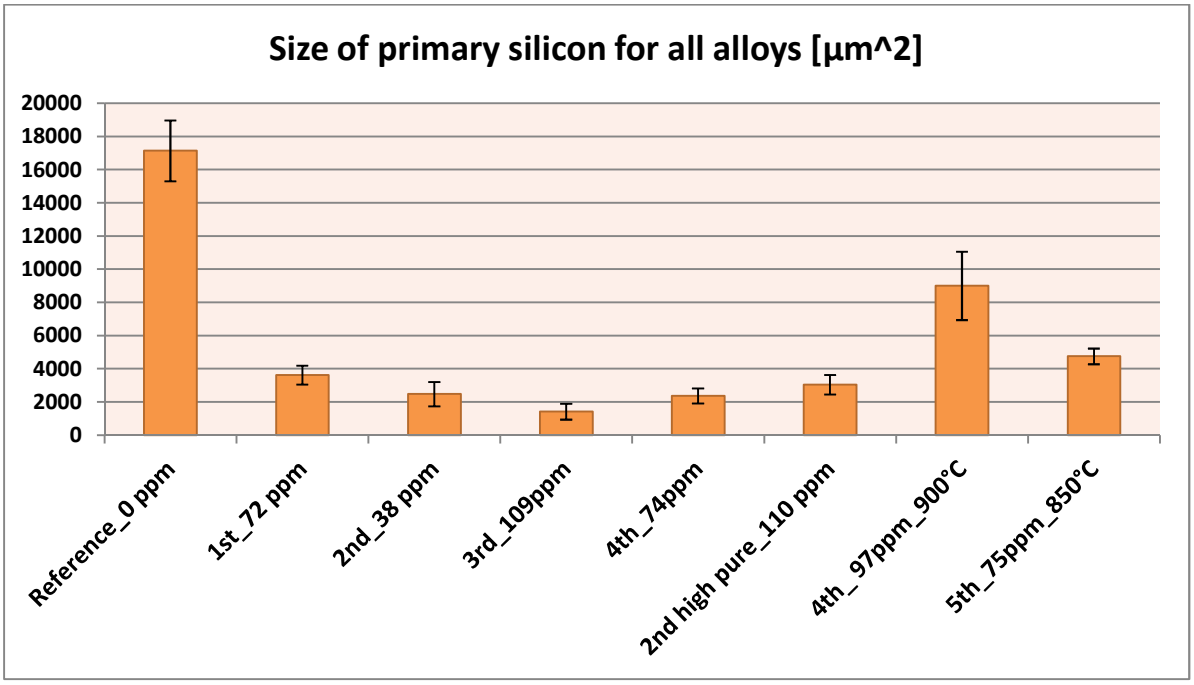

Figure 45 Data overview with all alloys

Comparing all the alloys together the meaning of the experiments is not clear. First of all the presence of the phosphorus impurities inside the commercial raw material was found, so it means that other not-checked impurities , as iron, might be inside the alloy. The iron, for example, is another element that can give to the silicon some nucleation sites, as the phosphorus, so the refinement in the commercial alloy is due to the phosphorus but it might be due to the iron (or other impurities) . The results have more sense if they are compared in two different sections: commercial alloys and high pure alloys.

From fig. 45, it can be seen that the alloy made of high purity metals with addition of 110 ppm P has even larger size of primary Si particles than the alloy made of commercial purity metals with addition of 109 ppm P. It implies that the primary Si particles are easier to refine in the alloys with a higher content of impurities.

By comparing alloys casted with the same temperature, some aspects might be clearer:

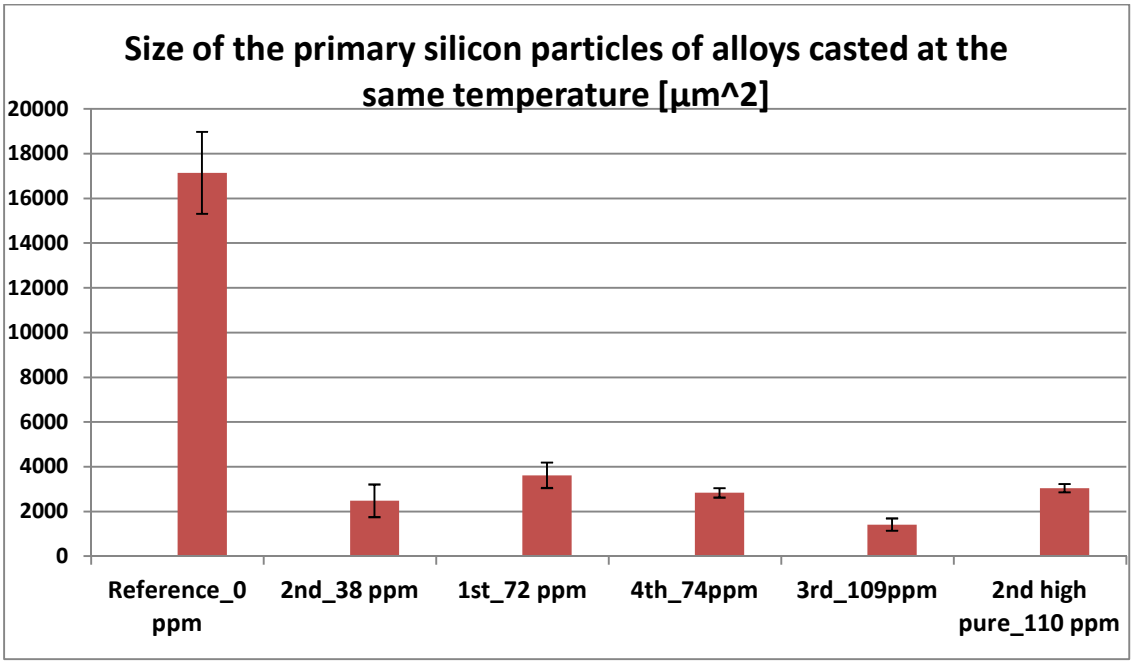

Figure 46 Size of the primary silicon particles of the alloys casted from the same temperature

And then finally the comparison between only commercial alloy:

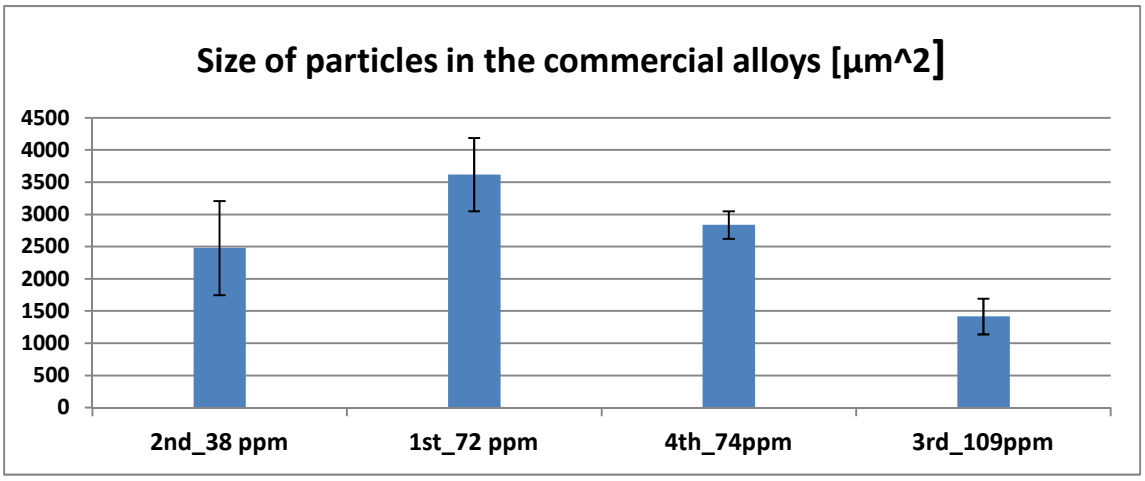

Figure 47 Size of primary silicon particles in the commercial alloys

As regards the commercial alloys the best grain refinement occurs at the highest level of phosphorus (3rd alloy with 109 ppm of phosphorus). Although this is in accordance with what was expected, the data are compatible within a small range, so the role of phosphorus is not clear comparing the data of the 1st, 2nd, 3rd and 4th alloy. This was one of the reasons why another casting was done.

Focusing on the role of the holding and casting temperature, from fig.45 the effect is clearer; increasing the holding temperature the silicon particles are getting bigger, then the phosphorus effect is frustrated. This is due to three reasons:

- The phosphorous is a very volatile element, so, increasing the temperature a part of it might go away; anyway this reason is the least important one because the chemical analysis were done after the casting experiments.
- By increasing the temperature the mobility of the particles increases as well, then the phosphorous has the possibility to agglomerate together giving to le liquid less but bigger nucleation sites.
- In order to reach an higher temperature, the liquid was kept at high temperature for a longer time so as the phosphorous had more time to agglomerate.

Thus, for the commercial alloy the role of the phosphorous is less important than the role of the casting temperature.

As regards the alloys with high pure raw material, the effect of the phosphorous is more evident; the differences are in terms of size and shape. The sizes, as it was expected, is almost 8 times smaller (fig.46) in the modified alloy, and in these alloys, this effect is only due to the phosphorous because there are not other impurities inside. Furthermore the silicon particles are better spread in the aluminum matrix because the particles of phosphorus give to the alloy more and equal spread sites for the nucleation, and the result is an alloy with really good mechanical proprieties, with less critical trigger crack point.

Comparing the shape of the particles among the modified and the unmodified alloy, the difference is well-clear: in the unmodified one the particles have a star-like shape and they are very irregular and angular; it means that there are a big amount of preferential trigger crack points especially on the border of the particles. Even during the sample preparation for the X-ray machine, the samples were more brittle than the modified alloys, and this was why the liquid nitrogen was used: as soon as the sample was touched with the normal tools for the mechanical remove from the support it broke. When looking at the modified alloy the shape of the particles here is more regular with a polygon shape; the angles of the shapes are less acute, so the particles, instead of becoming a preferential trigger crack point, they might be a stop crack points. This is also due to the good spread of them inside the matrix.

5.3.2 Floating effect

By using a light microscope, some macro segregation effects were clearly observed. These are due to the floating effect, that is particularly evident in these alloys because of the amount of copper which increases the density of the liquid. The following images show the macro segregation caused by the floating of Si crystals.

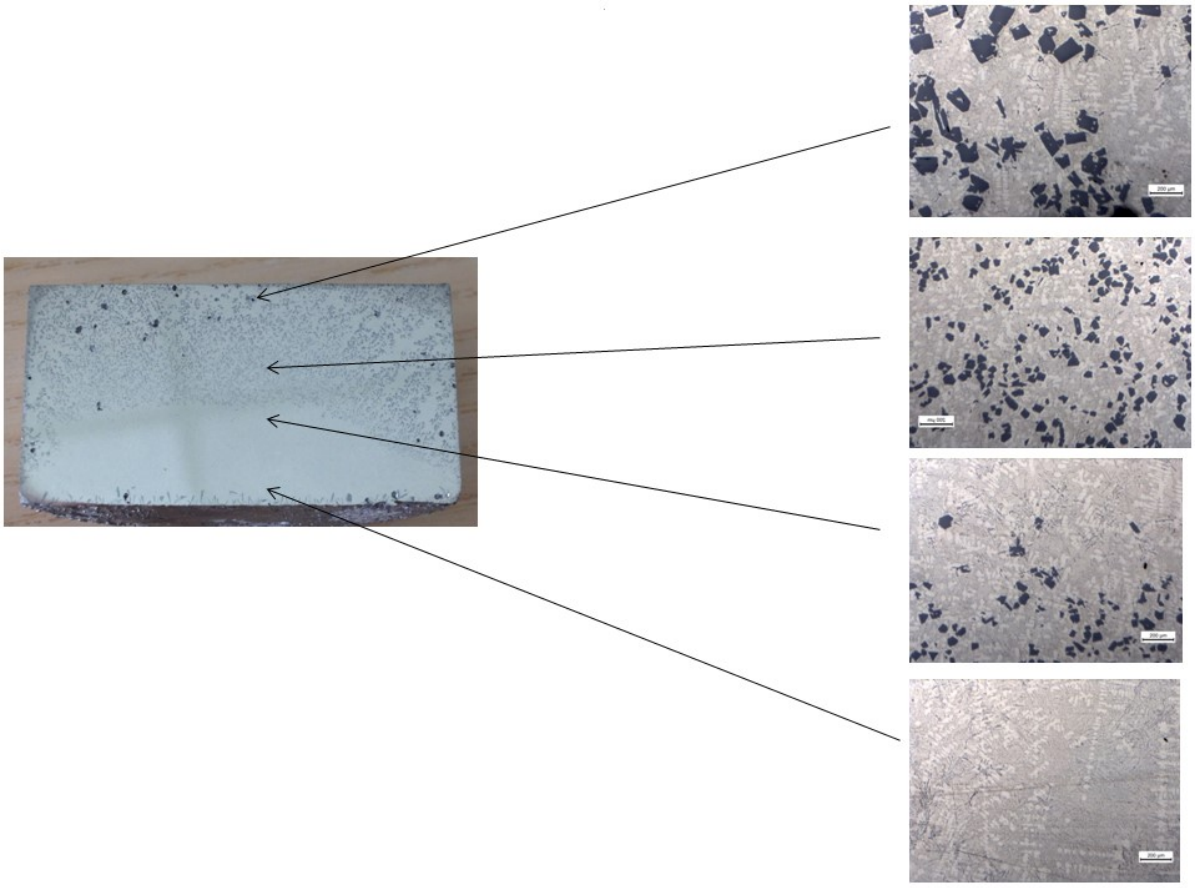

Figure 48 Sample with different pictures taken from the bottom to the top

This effect might be dangerous for the data acquisition, because if the pictures had not been taken in the same part of the samples the data might be affected. Fortunately the floating was recognized at the beginning.

This occurs because of the high difference of density among the liquid and the primary solid phase (silicon), and this is due to the high amount of copper in the liquid. This, during the solidification process, leads the silicon to float. Fortunately, using the cooling rate that was used (1,2 K/s), the problem was partially avoided because the particles formed were small; moreover for the modified alloy the problem was less evident because the particles were smaller thanks to the phosphorous. Anyway the floatation makes the micro-structure of the sample uneven, with big particles on the top, smaller in the middle and even no primary silicon at the bottom. For our test, as it

has been said previously, the data are almost not affected by the flotation because all the pictures were collected in the same spots of the sample.

The flotation might be important for the industrial application; although the copper is not used in the commercial Al-Si hypoeutectic alloys, the flotation occurs also in a only aluminum liquid though the difference of density among aluminum and silicon is lower. Thus, the casting with these alloys, are applicable for artifacts which are not huge, because in the middle of them, the cooling rate is lower than in the border, so the liquid takes more time to solidify and the segregation occurs.

5.4 Image sequences of in-situ X-ray radiographic study

In this part the solidification sequence of different alloys was recorded as videos. There are also some good pictures collected , where size difference and the number of the nucleation sites are clear shown. As it has been said before, the experiments were done with four different cooling rates.

The experiments were done only for the alloy with high pure raw material. The reason why this happened was because, for the commercial alloys the differece, in terms of nucleation sites, was not evident as between the high pure alloys. This is because, for the small area analyzed, it is difficult to understand if there are more or fewer particles. Anyway this experiments was done in order to see and film how the particles growth and the differences between the unmodified and the modified one.

With cooling rate set as 0.025 K/s:

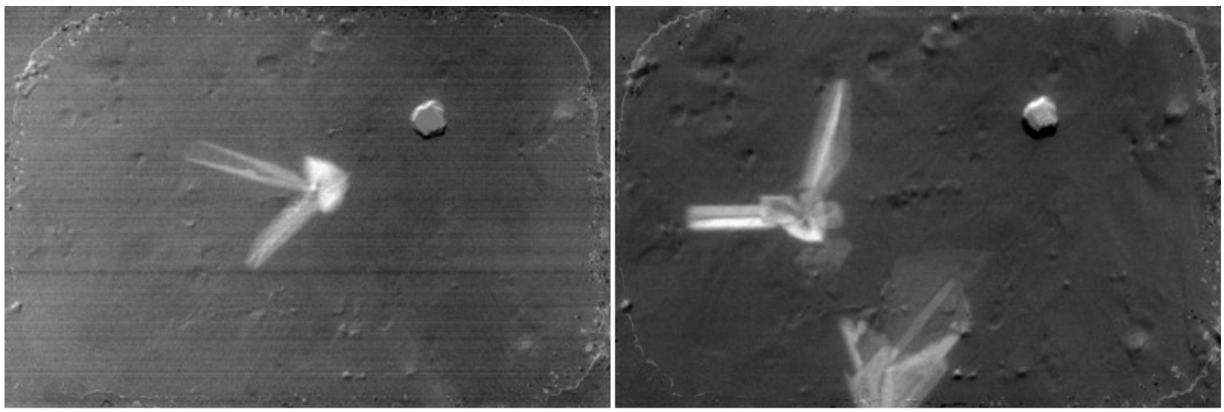

Figure 49 Reference Al-20Cu-18Si alloy (0ppm P) at 0.025 K/s

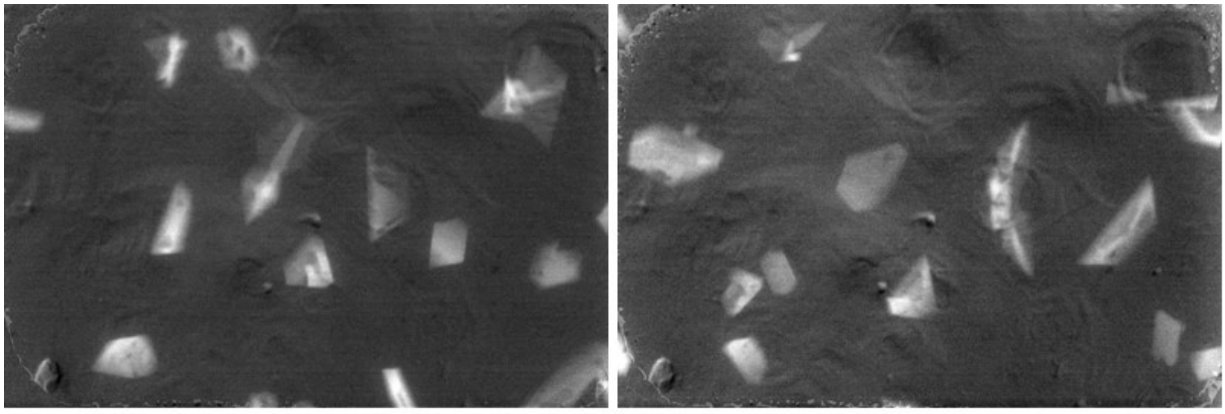

Figure 50 Al-20Cu-18Si alloys made of high purity Al and Cu with 110 ppm of P, cooling rate:0.025 K/s

With cooling rate set as 0.1 K/s:

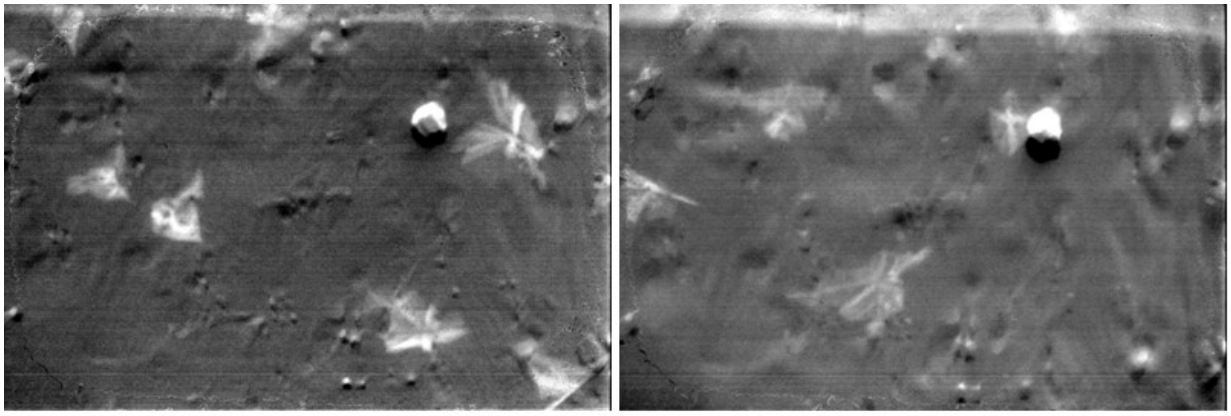

Figure 51 Reference Al-20Cu-18Si alloy (0ppm P) at 0.1 K/s

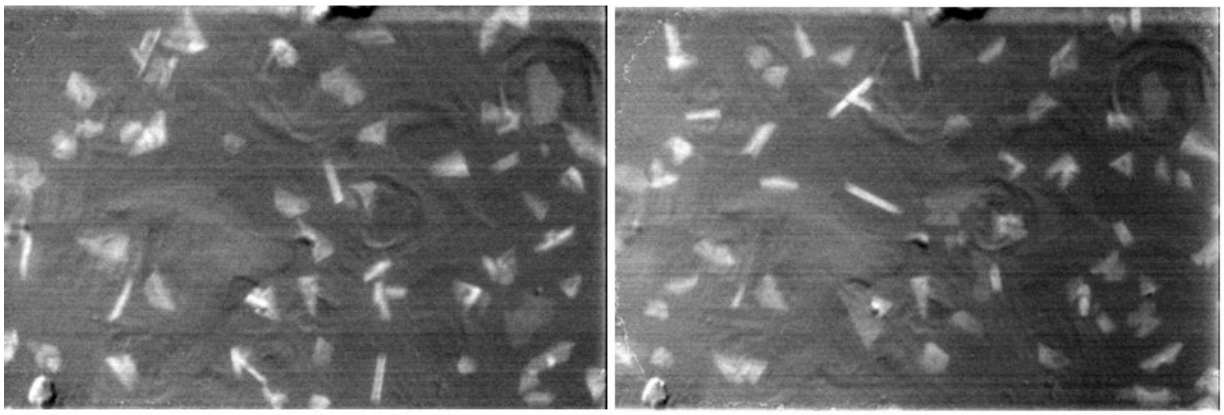

Figure 52 Al-20Cu-18Si alloys made of high purity Al and Cu with 110 ppm of P at 0.1 K/s

With cooling rate set as 0.5 K/s:

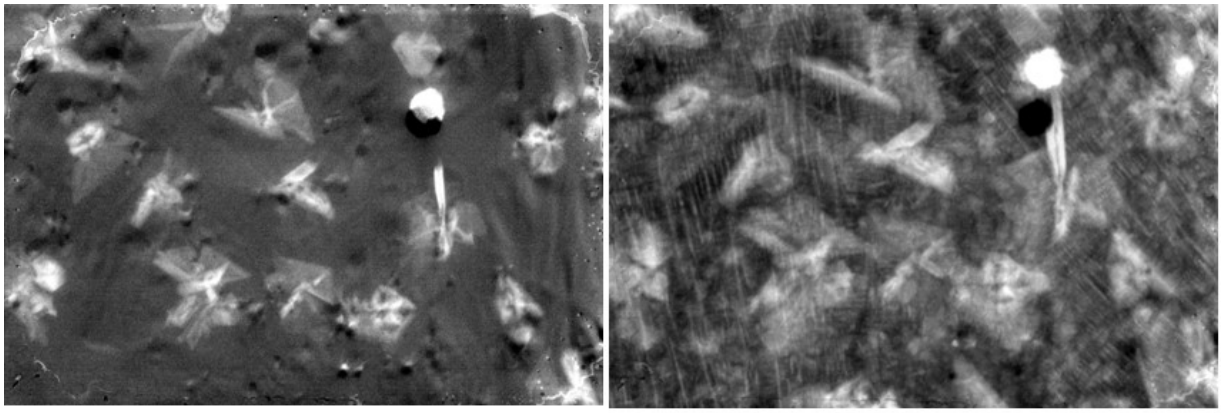

Figure 53 Reference Al-20Cu-18Si alloy (0ppm P) at 0.5 K/s, with the eutectic phase in the right picture

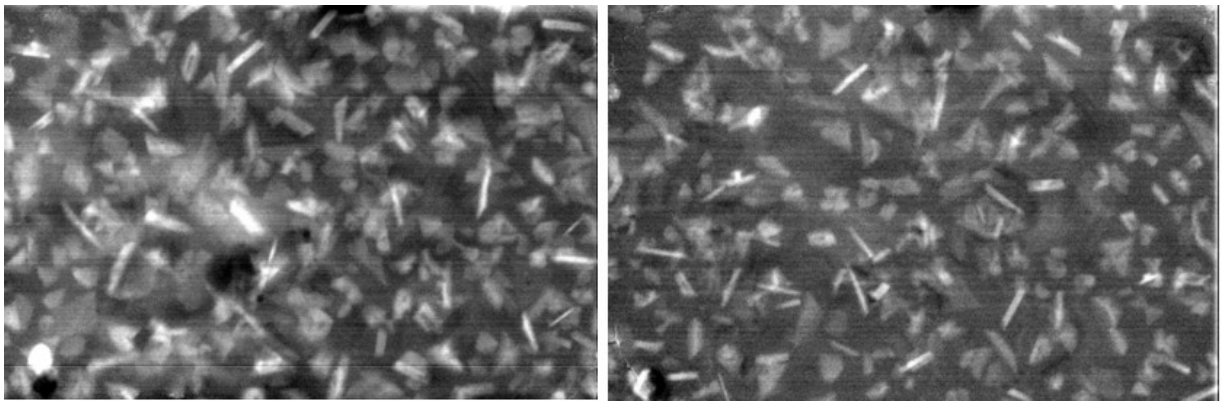

Figure 54 Al-20Cu-18Si alloys made of high purity Al and Cu with 110 ppm of P at 0.5 K/s

At last the highest cooling rate, the same of the casting experiment, 1.2 K/s:

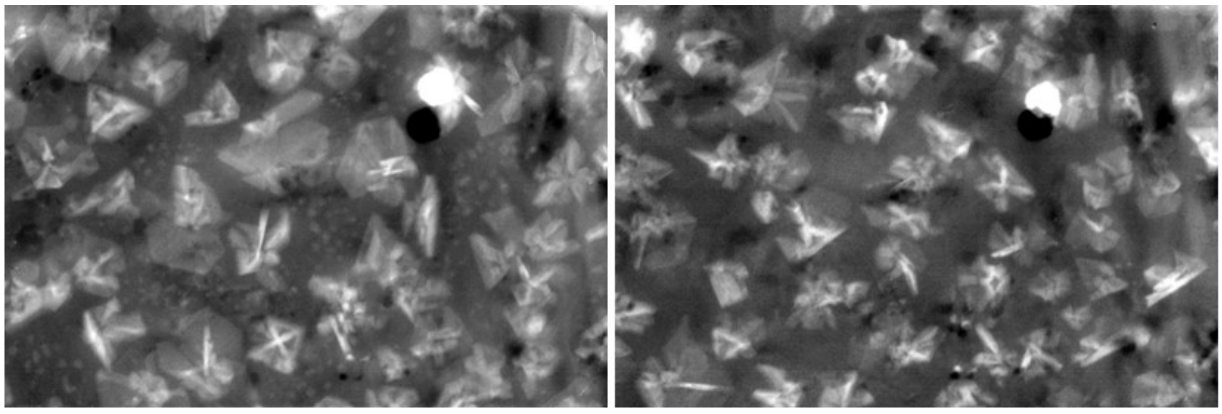

Figure 55 Reference Al-20Cu-18Si alloy (0ppm P) at) at 1.2 K/s

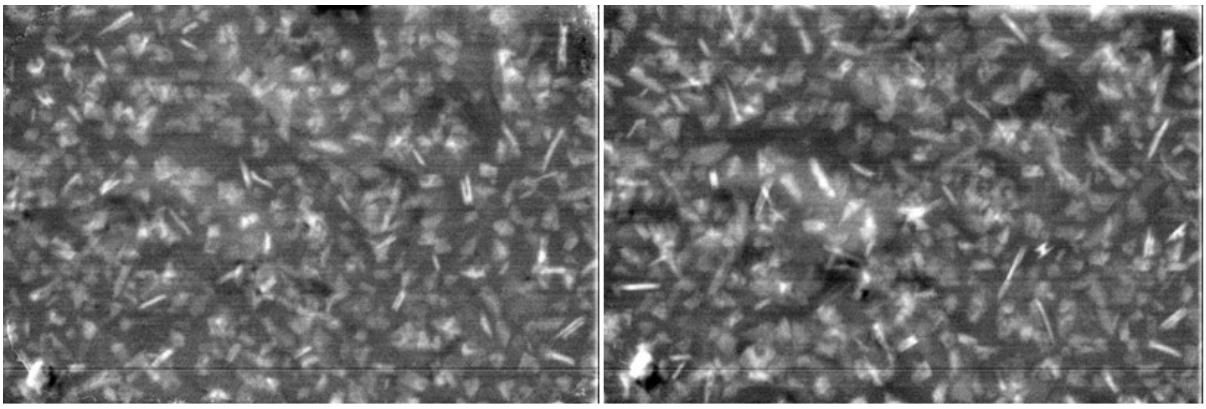

Figure 56 Al-20Cu-18Si alloys made of high purity Al and Cu with 110 ppm of P at 1.2 K/s

Starting from the unmodified alloy, in the videos it is possible to see the process: prefacing that each experiments (with different cooling rate) was done twice, every time the nucleation sites changed, so that there were no sites in the furnace as preferential nucleation sites, which might be distort the data. Then when the particles start to grow, they have grown in different directions, giving some star-like in the alloy, as it was previously seen. The particles were fewer, just a couple (at the lowest cooling rate) in the area filmed. Obviously increasing the cooling rate the number of particles increase. The interesting point is that, this increase is more evident with the modified alloy, and in fig.58 it is possible to see this difference, checking the different slopes of the curves. As regards the eutectic point, it is not influenced by the modification, and in the video it is interesting to see the solidification front coming from the coldest part (the top) and crossing the whole sample.

The modified alloy shows the differences mostly at high cooling rate; from fig.56 it is clear the action of phosphorous, because the particles are well spread giving to the alloy an uniform matrix. The refinement is more clear when the cooling rate increases arriving close to the normal cooling rate in the commercial application. Also here the nucleation sites changed every time, so there were no preferential nucleation sites, but only the phosphorous particles.

During the solidification process, thanks to the two thermocouples inside the furnace, the temperature was collected in order to see the right point of the nucleation start. This step was done by watching picture by picture in every video, checking when the first Si particle appeared, and then reading the temperature that was associated with this shot. It has been found that the nucleation temperature changes with the changing of the amount of phosphorus added and the cooling rate, as shown in the following graph:

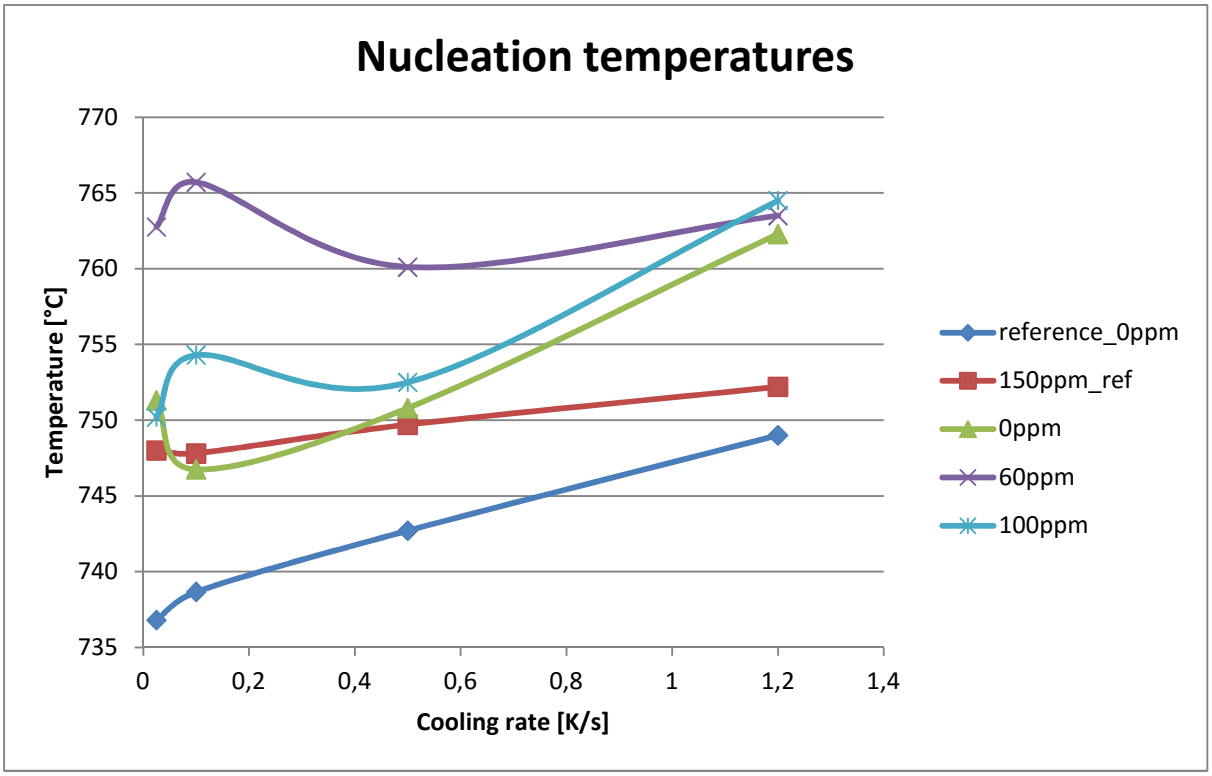

Figure 57 Nucleation temperatures of the different alloys

The number of primary Si particles were also analyzed. Since the sharpness of some of the pictures is poor, it was difficult to accurately measure the particle size. However, it is more reliable and easier to get the number of particle per image. Moreover it can give a real view of the phosphorus effect. The following graph shows the number of nucleation site (particles) in each alloy in every cooling rate:

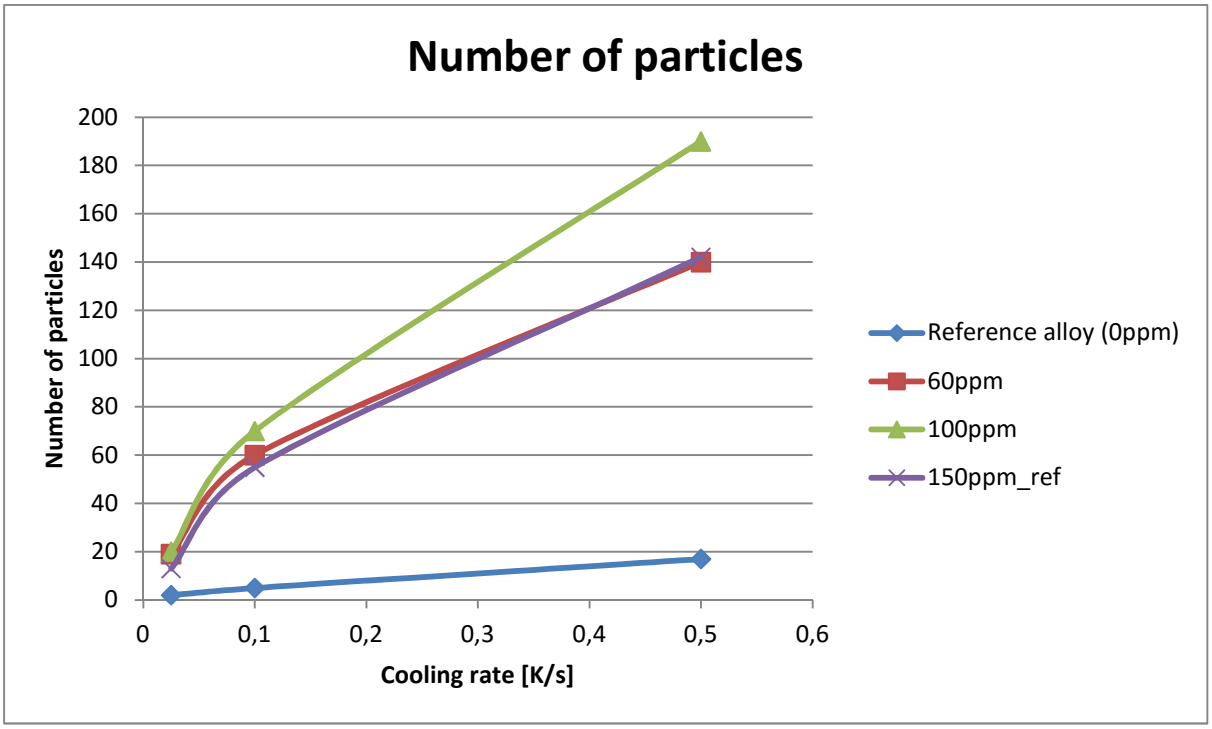

Figure 58 Number of particles in the different alloys with different cooling rates.

6 Conclusion

After this big amount of experiments some conclusions are obtained:

- The holding temperature has an important role in the primary silicon refinement. As it has been said previously, by increasing the holding temperature the phosphorus effect is getting worse and worse. It means that, if an high temperature casting is required, the modification is not possible with phosphorus and another refiner has to be used. The high casting temperature is required when the mold is difficult to fill, because of the shape of the final artifact; during the filling, if there is a complicated part to fill, the alloy might be solidified before the completed filling, so an high casting temperature is compulsory. Thus, the phosphorus modified alloys are good when the final shape of the artifact in not complicated or it is not too big.
- The commercial alloys have some impurities inside. If we want to be sure that the alloy is not over saturated of phosphorous we should start from high pure raw materials. Thus, the process is becoming expensive if the artifact is huge because it requires a lot of material. Then, also here, it is clear that the modification with phosphorus give better results for small artifact.
- The flotation here was more evident because of the copper. But also without copper, the silicon floats, giving an uneven microstructure. It means that for the commercial fields some precautions have to be observed in order to avoid

the problem: first of all using an high cooling rate the particles cannot start to float because there is not enough time; this is possible mostly for small pieces, so there are more reasons to use this refinement way only for small pieces. If it necessary for a big artifact, the technology has to be changed using for example a rotational mold with low rotation speed. Anyway some segregation phenomena might occur.

- The phosphorous refinement is clearer when the cooling is increased. Then it is better, once again, to use this technique for small pieces. Furthermore if inside the mold there is a cooling rate gradient, as happens with big mold, the difference between the microstructure increases also for this reason as well as for the cooling rate. Anyway in order to exploit the modification it is better to use an high cooling rate, such as 1,2 K/s.

Bibliography

1. Metallizazione sul silicio, Diego Colombo.
2. Crystal growth of the primary silicon in an A1-16 wt % Si alloy K. Kobayashi, P. H. Shingu, R. Ozaki, Department of Metal Science and Technology, Kyoto University, Kyoto, Japan.
3. Growth structures in aluminium-silicon alloys o.a. atasoy, F. Yilmaz and R. Elliot Department of Metallurgy, University of Manchester (UMIST), Manchester Ml 7HS, UK.
4. Notes and slide of metallurgical industrial applications, F. Bonollo.
5. Hypereutectic aluminum and silicon alloys Raymond J. Donahue, Fond du Lac; G. Hester-berg, Rosendale;Terrance M. Cleary, Allentown, all Of Wis.
6. Computer Aided Cooling Curve Analysis and Microstructureof Cerium Added Hypereutectic Al–Si (LM29) Alloy V. Vijeesh • K. Narayan Prabhu.
7. Grain Refinement of Commercial ECGrade 1070 Aluminium Alloy for Electrical Application, Massoud Hassanabadi.
8. Influences of complex modification of P and RE on microstructure and mechanical properties of hypereutectic Al-20Si alloy.
9. The synthesis of novel powder master alloys for themodification of primary and eutectic silicon crystals. A.V.Pozdniakov, M.V.Glavatskikh, S.V.Makhov , V.I.Napalkov.
10. “Series of Al–P Master Alloy and excellent refining performance on hypereutectic A390 Alloys”. Zuo Min , Liu Xiangfa.
11. New Approaches to Casting Hypereutectic Al-Si Alloys to Achieve Simultaneous Refinement of Primary Silicon and Modification of Eutectic Silicon “ Kawther W. A. Al-Helal”.

12. Ullah, M.W., Carlberg, T., *Silicon Crystal Morphologies during Solidification Refining from Al-Si Melts.* The 16th International Conference on Crystal Growth (ICCG16)/The 14th International Conference on Vapor Growth and Epitaxy (ICVGE14), 2011. **318**(1): p. 212-218.
13. Xu, C.L., Jiang, Q. C., *Morphologies of Primary Silicon in Hypereutectic Al-Si Alloys with Melt Overheating Temperature and Cooling Rate.* J. Mater. Sci. Eng. A, 2006. **437**(2): p. 451-455.
14. An Overview of the Development of Al-Si-Alloy Based Material for Engine Applications *"Haizhi Ye".*
15. Modern experimental methods for surface and thin-film chemical analysis, Charles A. Evans, Jr., Richard J. Blattner.
16. New investigation of phase equilibria in the system Al–Cu–Si.
17. GE Inspection Technologies, Industrial Radiography, Image forming techniques
18. Compact x-ray microradiograph for in situ imaging of solidification. processes:Bringing in situ x-ray micro-imaging from the synchrotron to the laboratory C. Rakete, C. Baumbach, A. Goldschmidt, D. Samberg, C. G. Schroer,1F. Breede, C. Stenzel,2 G. Zimmermann, C. Pickmann, Y. Houltz, C. Lockowandt, O. Svenonius, P. Wiklund, and R. H. Mathiesen.